senSCOPE: Modeling radiative transfer and biochemical processes in mixed canopies combining green and senescent leaves with SCOPE

Javier Pacheco-Labrador[1], Tarek S. El-Madany[1], Christiaan van der Tol[2], M. Pilar Martin[3], Rosario Gonzalez-Cascon[4], Oscar Perez-Priego[5], Jinhong Guan[6], Gerardo Moreno[7], Arnaud Carrara[8], Markus Reichstein[1] and Mirco Migliavacca[1].

[1]Max Planck Institute for Biogeochemistry, Hans Knöll Straße 10, Jena, D-07745, Germany
[2]Faculty of Geo-Information Science and Earth Observation (ITC), University of Twente, PO Box 217, AE Enschede 7500, The Netherlands
[3]Environmental Remote Sensing and Spectroscopy Laboratory (SpecLab), Institute of Economic, Geography and Demography (IEGD-CCHS), Spanish National Research Council (CSIC), C/Albasanz 26-28, 28037 Madrid, Spain
[4]Department of Environment, National Institute for Agriculture and Food Research and Technology (INIA), Ctra. Coruña, Km. 7,5, 28040 Madrid, Spain
[5]Department of Biological Sciences Macquarie University, 6 Wally's Walk, NSW 2109, Australia.
[6]State Key Laboratory of Soil Erosion and Dryland Farming on the Loess Plateau, Northwest A&F University, Yangling, Shaanxi 712100, China
[6]Forest Research Group - INDEHESA University of Extremadura, 10600 Plasencia, Spain
[7]Fundación Centro de Estudios Ambientales del Mediterráneo (CEAM), Charles Darwin 14, Parc Tecnològic, 46980 Paterna, Spain

Correspondence to: Javier Pacheco-Labrador (jpacheco@bgc-jena.mpg.de)

Abstract.

Semi-arid grasslands and other ecosystems combine green and senescent leaves featuring different biochemical and optical properties, as well as functional traits. Knowing how these properties vary is necessary to understand the functioning of these ecosystems. However, differences between green and senescent leaves are not considered in recent models representing radiative transfer, heat, water and CO_2 exchange such as the Soil-Canopy Observation of Photosynthesis and Energy fluxes (SCOPE). Neglecting the contribution of senescent leaves to the optical and thermal signal of vegetation limits the possibilities to use remote sensing information for studying these ecosystems; as well as neglecting their

lack of photosynthetic activity increases uncertainty in the representation of ecosystem fluxes. In this manuscript we present senSCOPE as a step towards a more realistic representation of mixed green and senescent canopies. senSCOPE is a modified version of SCOPE model that describes a canopy combining green and senescent leaves with different properties and function. The model relies on the same numerical solutions than SCOPE, but exploits the linear nature of the scattering coefficients to combine optical properties of both types of leaf. Photosynthesis and transpiration only take place in green leaves; and different green and senescent leaf temperatures are used to close the energy balance. Radiative transfer of sun-induced fluorescence (SIF) and absorptance changes induced by the xanthophyll cycle action are also simulated. senSCOPE is evaluated against SCOPE both using synthetic simulations, forward simulations based on observations in a Mediterranean tree-grass ecosystem, and inverting dataset of ground measurements of reflectance factors, SIF, thermal radiance and gross primary production on a heterogeneous and partly senescent Mediterranean grassland. Results show that senSCOPE outputs vary quite linearly with the fraction of green leaf area, whereas SCOPE does not respond linearly to the effective leaf properties, calculated as the weighted average of green and senescent leaf parameters. Inversion results and pattern-oriented model evaluation show that senSCOPE improves the estimation of some parameters, especially chlorophyll content, with respect SCOPE retrievals during the dry season. Nonetheless, inaccurate knowledge of the optical properties of senescent matter still complicates model inversion. senSCOPE brings new opportunities for the monitoring of canopies mixing green and senescent leaves, and for improving the characterization of the optical properties of senescent material.

1 Introduction

Consistent monitoring of relevant vegetation properties is an essential step towards understanding the response of vegetation function (e.g., photosynthesis, transpiration) to changes in environment. Among others, photosynthetic performance and water use efficiencies are key elements to predict and understand vegetation responses to the climate change scenarios (e.g., elevated atmospheric CO_2 concentration, higher temperatures and altered water regimes) (IPCC 2014). However, current Land

Surface Models (LSM) predictions of these fluxes include large uncertainties (Friedlingstein et al. 2014); partly due to inadequate representation of different processes as well as to the lack of knowledge of functional parameters describing plant function (e.g., maximum carboxylation rate (V_{cmax}), maximum electron transport rate (J_{max}) or the Ball-Berry stomatal sensitivity (m)) (Rogers 2014; Rogers et al. 2016; Schaefer et al. 2012). Recent efforts of the Remote Sensing (RS) community have focused on the estimation of these parameters either using statistical approaches (Serbin et al. 2015; Silva-Perez et al. 2018), or combining Radiative Transfer Models (RTM) with Soil-Vegetation-Atmosphere Models (SVAT) (Bayat et al. 2018; Camino et al. 2019; Dutta et al. 2019; Pacheco-Labrador et al. 2019; Zhang et al. 2014; Zhang et al. 2018), notably using the Soil-Canopy Observation Photosynthesis and Energy fluxes (SCOPE) model (van der Tol et al. 2009).

SCOPE represents radiative transfer of optical and thermal infrared radiation (TIR), in a homogeneous 1-D canopy, which is coupled with an energy balance and a photosynthesis models predicting heat and water fluxes and carbon assimilation. SCOPE also propagates leaf level sun-induced chlorophyll fluorescence (SIF) emission and absorptance changes related with the activation of the xanthophyll cycle (Vilfan et al. 2018) to top of the canopy radiances. SCOPE uses Fluspect to model leaf optical properties (Vilfan et al. 2016; Vilfan et al. 2018) and combines 4 different canopy RTM representing outgoing radiation (RTM_o), SIF (RFM_f, (van der Tol et al. 2016)), TIR emission (RTM_t) and xanthophyll absorption (RTM_z, (Vilfan et al. 2018)) that rely on the four stream SAIL extinction and scattering coefficients model (Verhoef 1984). In addition, Yang and colleagues (2017) developed mSCOPE, an extension of SCOPE that uses a different numerical solution of the radiative transfer problem to represent 1-D but vertically heterogeneous canopies.

A current limitation of SCOPE is the lack of representation of within-canopy heterogeneity of vegetation properties, and specifically the separation of green and senescent leaves, which feature large differences in biophysical properties and function. When leaves senesce, flavonoids undergo enzymatic oxidation processes within the leaf producing diverse semiquinones and quinones which can suffer non-enzymatic secondary reactions with phenols, amino acids and proteins or other polyphenols (Pourcel et al. 2007; Taranto et al. 2017). The result is a heterogeneous mixture of complex brown polymers,

difficult to characterize *in vivo* and responsible of the yellow and brown tones that these leaves exhibit (Guyot et al. 1996; Pourcel et al. 2007). The characterization of the optical properties of these "senescent" or "brown" pigments of leaves were addressed by Jacquemoud (1988) using albino corn leaves; however, the authors stated that the characterization had to be improved. In fact, the absorption coefficients currently used by Prospect are usually attributed to F. Baret, via personal communication (e.g., (Féret 2009)). Thus, the characterization of senescent pigments is not as thoroughly documented as for other pigments (Feret et al. 2008; Féret et al. 2017; Jacquemoud and Baret 1990; Vilfan et al. 2018), and their concentration is presented in arbitrary units due to the measurement technique used in their determination (Jacquemoud 1988). Also, when leaves further degrade their color changes (Kidnie et al. 2015), and some of their optical properties might vary with respect to those characterized and used by leaf-level RTM. For example, Melendo-Vega et al, (2018) suggested that overestimation of near infrared reflectance factors in a semi-arid grassland could be related to senescent material, and that this effect increased with its longevity.

Commonly used models such as PROSAIL (Jacquemoud et al. 2009), or more recently SCOPE, allocate all the pigments in a unique "effective" according to the averaged concentrations of the different leaves of the canopy. However, this approach does not adequately represent mixed canopies with varying fractions of green and senescent leaves. The presence of non-photosynthetic elements in the canopy has been already addressed in turbid medium RTM (Bach et al. 2001; Braswell et al. 1996; Wenhan 1993) and used to improve the estimation of biophysical parameters such as leaf area index (*LAI*) or chlorophyll concentration (C_{ab}) or the fraction of absorbed photosynthetically active radiation (Houborg and Anderson 2009; Houborg et al. 2009; Houborg and McCabe 2016; Wenhan 1993). However, senescent and green leaves do not only feature different optical properties, but also different physiological processes. For example, senescent leaves present little or no chlorophyll content (Hörtensteiner 2006; Whitfield and Rowan 1974) so that they do not assimilate CO_2 through photosynthesis. Also, senescent leaves do not transpire water and lack of stomatal regulation. Senescent leaves can pose problems for the retrieval of biophysical variables if not adequately represented (Bacour et al. 2002; Houborg and Boegh 2008; Wang et al. 2005). Analogously, inadequate representation of

green and senescent leaf pools could also potentially induce uncertainties in the simulation of processes at canopy scale related to photosynthesis and transpiration. Finally, given that SCOPE is now widely used for retrieval of functional properties (Bayat et al. 2018; Camino et al. 2019; Dutta et al. 2019; Pacheco-Labrador et al. 2019; Zhang et al. 2014; Zhang et al. 2018), these uncertainties can propagate in the estimated parameters (Pacheco-Labrador et al. 2019). This fact may limit the application of recent approaches combining RTM and SVAT models for the study of canopies or ecosystems featuring large fractions of dry leaves (in particular in grasslands or semi-arid ecosystems) or for the monitoring of vegetation health, crop productivity and phenology.

Senescent material is present in all vegetation, and for a remote sensing perspective is very critical for annual plants such as grasslands (Houborg et al. 2009; Melendo-Vega et al. 2018), which cover about 40% of the Earth's terrestrial surface (Anderson 2006). Grassland's phenology and function are strongly governed by water availability, temperature, herbivory, fire, nitrogen deposition or CO_2 concentration increase (Anderson 2006; Cleland et al. 2006; Figueroa and Davy 1991; Luo et al. 2018; Migliavacca et al. 2011; Richardson et al. 2013). Green plants transit to senescent, recently dead, and long-term dead plants, each of them featuring different biophysical and optical properties (Kidnie et al. 2015). This transition varies with meteorology (Ren and Zhang 2018), biophysical properties (Henry et al. 2008; Sanaullah et al. 2010; Yuan and Chen 2009), plant functional types (Henry et al. 2008) and changes for different parts of the plant (Henry et al. 2008; Koukoura et al. 2003). Usually, even in grasses, leaves fall while stems stay longer and degrade more slowly due to differences in biochemical composition. Therefore, in multi-species grasslands senescence and degradation can take place at different rates and periods, increasing the variability of surface biophysical and optical properties as well as the complexity of modeling and characterization. In fact, senescent material and litter are nowadays considered a challenge for the estimation of biophysical properties in semi-arid grasslands (He and Mui 2010).

In this work, we present senSCOPE, a modified version of the SCOPE model that separates RTM and physiological processes (photosynthesis and transpiration) for green and senescent leaves. senSCOPE aims at improving the representation of radiative transfer and physiology in senescent canopies. The model is then evaluated in three ways:

1) We run a sensitivity analysis comparing forward simulations of SCOPE and senSCOPE under different meteorological conditions and under different combinations of vegetation parameters for different abundances of senescent leaves.

2) We use observations of model parameters and meteorological data at ecosystem scale to predict fluxes and compare them with EC data.

3) We invert SCOPE and senSCOPE against the same dataset of ground observations of carbon fluxes, reflectance factors (*R*), SIF and TIR radiance used by Pacheco-Labrador et al, (2019) for comparison.

As in the former work, functional and biophysical model parameters are estimated by inverting SCOPE against different combinations of the abovementioned variables sampled at plot scale in a Mediterranean grassland. New inversion boundaries are used according to observations of some of the parameters in the site. Results of both inversions are compared and evaluated using pattern-oriented model evaluation approach (Pacheco-Labrador et al. 2019).

2. Description of senSCOPE

The model senSCOPE extends the 1-D model SCOPE to describe homogeneous canopies combining green and senescent leaves randomly mixed. Fig. 1 summarizes the conceptual differences between SCOPE and senSCOPE. Green leaves contain chlorophylls and other photosynthetic pigments that allow them to photosynthesize; and regulate their temperature via transpiration. In contrast, senescent leaves only contain senescent pigments and neither photosynthesize nor transpire. These leaves present some microbial activity related to its degradation, and superficial water (e.g., intercepted rainfall) can evaporate from their surface; however these processes are not represented neither by SCOPE nor senSCOPE. In senSCOPE, the leaf RTM Fluspect (Vilfan et al. 2016; Vilfan et al. 2018) simulates reflectance, transmittance and, in the case of green leaves, also fluorescence according to the biochemical and structural properties of each leaf type. Canopy RTM_o implemented in SCOPE (van der Tol et al. 2009) is modified to separately compute the radiation absorbed by each leaf type; and the

energy balance model is customized to account for the presence of leaves that neither photosynthesize nor transpire. Since green and senescent leaves feature different radiative balances, a modified RTM_t model quantifies thermal emission of each of these two leaf types separately and combines them according to the corresponding fractions of leaf area (*f*); then the model calculates scattering and absorption of this diffuse flux. Eventually, fluorescence emission and optical changes induced by the activation of the xanthophyll cycle in the green leaves is propagated to top of canopy (TOC) radiances and *R* using the RTM_f (van der Tol et al. 2016) and RTM_z (Vilfan et al. 2018) models already implemented in SCOPE. Both models are coded in Matlab (Matwoks Inc., Natick, MA, USA).

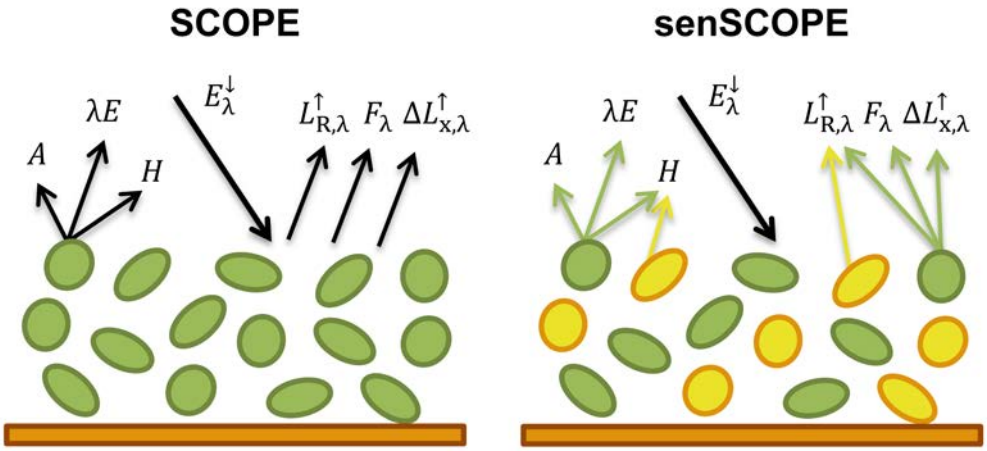

Figure 1. Conceptual differences between SCOPE and senSCOPE models. Green and yellow colours correspond to green and senescent leaves, respectively. Black arrows show processes featured by all leaves; whereas coloured arrows refer to processes featured only for a given type of leaf. The scheme represents assimilation (*A*), latent (λE) and sensible heat (*H*) fluxes, incoming spectral irradiance (E_λ), reflected spectral radiance ($L_{R,\lambda}$), emitted fluorescence radiance (F_λ) and changes in $L_{R,\lambda}$ due to activation of xanthophyll cycle ($\Delta L_{x,\lambda}$)

senSCOPE relies on the same solution of the radiative transfer problem implemented in SCOPE, since it exploits the linear nature of the single leaf scattering efficiency factors (Verhoef 1984) to combine the optical properties of green and senescent leaves in an "averaged" leaf. This is simple if leaf angle distribution is assumed the same for both types of leaves. The main advantage of this approach is that it allows representing physiological processes separately in each leaf type. This is important since photosynthesis and transpiration are non-linearly related with radiation and leaf temperature, and

184 therefore might not be adequately represented by a model featuring a unique leaf type characterized by
185 the "averaged parameters" of photosynthetic and non-photosynthetic leaves.

186 senSCOPE requires a larger number of parameters than SCOPE, since two different leaves must be
187 described, as well as their respective area fractions. Alternatives to minimize the number of parameters
188 and simplify the application of the model in inverse problems are presented in Sect. 3.2.2 and discussed
189 later.

190 **2.1 Radiation Fluxes**

191 As SCOPE, senSCOPE relies on SAIL 4-stream theory that can be summarized by a system of four
192 linear equations describing the radiative transfer of the solar direct flux (E_s), the downward diffuse flux
193 (E^-), the upward diffuse flux (E^+), and the flux in the observation direction (E_o).

194 $$\frac{dE_s}{Ldx} = kE_s \,, \tag{1a}$$

195 $$\frac{dE^-}{Ldx} = -sE_s + aE^- - \sigma E^+ \,, \tag{1b}$$

196 $$\frac{dE^+}{Ldx} = -s'E_s + \sigma E^- - aE^+ \,, \tag{1c}$$

197 $$\frac{dE_o}{Ldx} = wE_s + vE^- + v'E^+ - KE_o \,, \tag{1a}$$

198 In this system, x represents the vertical relative height within the canopy (x = 0 for top, x = -1 for
199 bottom), and L represents the Leaf Area Index (also *LAI*). The remaining variables are the SAIL
200 coefficients defined for first time by Verhoef (1984). k and K are the extinction coefficients in the solar
201 and observation directions, respectively. They depend on the sun-view geometry, *LAI* and the leaf angle
202 distribution (*LAD*); and they are therefore independent of leaf optical properties. s, a, σ, s', w, v and v'
203 are the scattering coefficients depending on sun-view geometry, canopy structure and leaf optical
204 properties. These coefficients define the relationship between a given incident flux (E_1) and a given
205 scattered flux (E_2) in the canopy, and they are computed by integrating single-leaf scattering efficiency
206 factors (Q_{sc}) that represent the analogous relationship for individual leaves. The scattering coefficient

(b) corresponding to all the leaves of given zenith inclination angle (θ_l) can be defined as (Verhoef 1984):

$$b(\theta_l) = \frac{L'}{2\pi}\int_0^{2\pi} Q_{sc}(E_1, E_2)d\varphi_l \,, \quad (2)$$

where L' is the *LAI* contained in a horizontal layer of the canopy of width dx and φ_l is the leaf azimuth angle.

As in SCOPE, senSCOPE solves the radiative transfer problem numerically, defining a discrete number of canopy layers and leaf angles. $Q_{sc}(E_1, E_2)$ are defined assuming that individual leaves are Lambertian diffusors of known hemispherical reflectance (ρ) as and hemispherical transmittance (τ). ρ and τ are predicted in SCOPE by Fluspect (Vilfan et al. 2016). For each pair of incident and scattered fluxes, $Q_{sc}(E_1, E_2)$ is defined as a linear combination of ρ and/or τ weighted by spectrally invariant factors determined by the geometry of the leaf, or more specifically, the projection of the leaves with respect to the incident flux (E_1) and the downward (-) or upward (+) scattered flux (E_2). As proposed by Bach et al, (2001), senSCOPE exploits this linear nature of Q_{sc} to combine the ρ and the τ of green and senescent leaves into an averaged factors; weighted by their corresponding fractions of leaf area (Eq. 3 and 4). This approach allows applying the solution already proposed by van der Tol et al., (2009) for the linear system shown in Eq. 1a-d.

$$\rho = f_{green}\rho_{green} + (1 - f_{green})\rho_{senes} \,, \quad (3)$$

$$\tau = f_{green}\tau_{green} + (1 - f_{green})\tau_{senes} \,, \quad (4)$$

where subscripts "green" and "senes" indicate the type of leaf. Notice that the weighted average of ρ and τ is not equivalent to the factors predicted for a weighted average of the leaf parameters.

This approach is suitable to represent the radiative transfer of a canopy of homogeneously mixed green and senescent leaves. In order to represent physiological processes for each leaf type separately, it is necessary differentiating the amount total radiation absorbed by each leaf type, and the photosynthetically active radiation (*PAR*) absorbed by chlorophyll ($E_{ap,Chl}$). SCOPE quantifies $E_{ap,Cab}$ (W m^{-2}) using the relative absorption of this pigment respect to the remaining total absorption in the leaf

in each spectral band ($k_{\mathrm{Chl,rel}}$). $E_{\mathrm{ap,Chl}}$ is computed for the direct ($E_{\mathrm{ap,Chl,dir}}$) and the diffuse irradiances ($E_{\mathrm{ap,Chl,dif}}$) as follows:

$$E_{\mathrm{ap,Chl,dir}} = f_{\mathrm{green}} \int_{\lambda=400}^{\lambda=700} k_{\mathrm{Chl,rel,green}}(\lambda) E_{\mathrm{sun}}(\lambda) \left[1 - \rho_{\mathrm{green}}(\lambda) - \tau_{\mathrm{green}}(\lambda)\right] d\lambda \,, \quad (5)$$

$$E_{\mathrm{ap,Chl,dif}}(x) = f_{\mathrm{green}} \int_{\lambda=400}^{\lambda=700} k_{\mathrm{Chl,rel,green}}(\lambda) [E^{-}(x,\lambda) + E^{+}(x,\lambda)] \left[1 - \rho_{\mathrm{green}}(\lambda) - \tau_{\mathrm{green}}(\lambda)\right] d\lambda, \quad (6)$$

where λ is the wavelength and $k_{\mathrm{Chl,rel,green}}$ is $k_{\mathrm{Chl,rel}}$ in the green leaves. These quantities are calculated from the upward and downward fluxes without modifying the transfer of radiation. Since senSCOPE defines senescent leaves as containing no chlorophyll, $k_{\mathrm{Chl,rel}} = 0$ in senescent leaves and for this reason, absorbed PAR used to simulate photosynthesis in sunlit ($E_{\mathrm{ap,Chl,u}}$) and shaded leaves ($E_{\mathrm{ap,Chl,h}}$) per total leaf area of the mixed canopy scales with f_{green}. Shaded leaves (subscript 'h') are only illuminated by diffuse light (Eq. 7); whereas Eq. 5 and 6 must be combined to get $E_{\mathrm{ap,Chl}}$ in the sunlit leaves ($E_{\mathrm{ap,Chl,u}}$, subscript 'u') (Eq. 8).

$$E_{\mathrm{ap,Chl,h}}(x) = E_{\mathrm{ap,Chl,dif}}(x) \,, \quad (7)$$

$$E_{\mathrm{ap,Chl,u}}(x,\theta_{\mathrm{l}},\varphi_{\mathrm{l}}) = |f_{\mathrm{s}}(x,\theta_{\mathrm{l}},\varphi_{\mathrm{l}})| E_{\mathrm{ap,Chl,dir}} + E_{\mathrm{ap,Chl,dif}}(x) \,, \quad (8)$$

where f_{s} is a geometric factor accounting for the projection of each leaf towards the sun.

Total absorbed radiation is used to compute the radiation budget in the canopy and determines leaf temperature, which has implications for photosynthesis and transpiration, and must therefore be computed separately for each leaf type. Total absorbed radiation is computed by SCOPE similarly as in Eq. 5-8, but integrating the fluxes in the full spectral domain (e.g., 400-50.000 nm):

$$E_{\mathrm{a},i,\mathrm{dir}} = f_{\mathrm{i}} \int_{\lambda=400}^{\lambda=50000} E_{\mathrm{sun}}(\lambda) [1 - \rho_i(\lambda) - \tau_i(\lambda)] \, d\lambda \,, \quad (9)$$

$$E_{\mathrm{a},i,\mathrm{dif}}(x) = f_{\mathrm{i}} \int_{\lambda=400}^{\lambda=50000} [E^{-}(x,\lambda) + E^{+}(x,\lambda)] \, [1 - \rho_{\mathrm{i}}(\lambda) - \tau_{\mathrm{i}}(\lambda)] d\lambda, \quad (10)$$

$$E_{\mathrm{a},i,\mathrm{h}}(x) = E_{\mathrm{a},i,\mathrm{dif}}(x) \quad (11)$$

$$E_{\mathrm{a},i,\mathrm{u}}(x,\theta_{\mathrm{l}},\varphi_{\mathrm{l}}) = |f_{\mathrm{s}}(x,\theta_{\mathrm{l}},\varphi_{\mathrm{l}})| E_{\mathrm{a},i,\mathrm{dir}} + E_{\mathrm{a},i,\mathrm{dif}}(x) \,, \quad (12)$$

Where subscript "*i*" now stands for either 'green' or 'senescent'.

2.2 Energy balance

As in SCOPE, energy balance is closed iteratively by modifying canopy and soil temperatures until the following is met for the soil and for all leaf angles and layers separately:

$$|R_{\mathrm{n}} - H - \lambda E - G| < \varepsilon_{\mathrm{threshold}}, \quad (13)$$

where R_{n} is net radiation, H is latent heat flux, λE is energy heat flux, G is soil heat flux and $\varepsilon_{\mathrm{treshold}}$ is a predefined threshold for the accepted energy balance closure error ($\varepsilon_{\mathrm{treshold}}$), all in W m^{-2}.

senSCOPE addresses the energy balance separating the processes occurring in green and senescent leaves, where only the first are assumed to photosynthesize and transpire. Therefore, $\varepsilon_{\mathrm{ebal}}$ is separated into the following elements (Eq. 14):

$$R_{\mathrm{n,green}} - R_{\mathrm{n,senes}} - R_{\mathrm{n,soil}} - H_{\mathrm{green}} - H_{\mathrm{senes}} - H_{\mathrm{soil}} - \lambda E_{\mathrm{green}} - \lambda E_{\mathrm{soil}} - G = \varepsilon_{\mathrm{ebal}}\,, \quad (14)$$

where the subscript "soil" refers to soil fluxes, and only green leaves and soil contribute to λE. However, notice that similarly as in SCOPE, the energy balance is separately closed for soil and for all leaf angles, layers and leaf types.

In order to compute R_{n}, the contribution of thermal emission must be added to the absorbed radiation calculated in Sect. 2.1. senSCOPE separately represents the temperatures of green and senescent leaves ($T_{\mathrm{c,green}}$, $T_{\mathrm{c,senes}}$, respectively) since they absorb radiation cool down differently. Distinguishing these temperatures has an impact on the calculation of photosynthesis, which is temperature dependent. Consequently, black-body thermal emission (H_{c}) is different for each leaf type ($H_{\mathrm{c,green}}$, $H_{\mathrm{c,senes}}$); and the on-sided black-body thermal emission of all leaves is computed as a linear combination of the emission of each leaf type in the canopy:

$$\varepsilon\, H_{\mathrm{c}} = f_{\mathrm{green}}\varepsilon_{\mathrm{green}}H_{\mathrm{c,green}}\left(T_{\mathrm{c,green}}\right) + \left(1 - f_{\mathrm{green}}\right)\varepsilon_{\mathrm{senes}}H_{\mathrm{c,senes}}\left(T_{\mathrm{c,senes}}\right), \quad (15)$$

where ε is the emissivity, and equals absorptance (1-ρ-τ) according to Kirchhoff's Law. The propagation of emitted radiation by leaves and soil through the canopy is calculated using the averaged layer properties as in the original SCOPE. In order to quantify the net thermal radiation (emitted minus

absorbed) ($R_{n,t}$) senSCOPE calculates the amount of energy absorbed by each leaf type using their respective emissivity:

$$R_{n,\mathrm{t,green}} = \left[E^- + E^+ - 2H_{\mathrm{green}}\right]\varepsilon_{\mathrm{green}} f_{\mathrm{green}} \,, \quad (16)$$

$$R_{n,\mathrm{t,senes}} = \left[E^- + E^+ - 2H_{\mathrm{senes}}\right]\varepsilon_{\mathrm{senes}}\left(1 - f_{\mathrm{green}}\right) \,, \quad (17)$$

where and E^- and E^+ are the diffuse emitted fluxes. $R_{n,t}$ of sunlit and shaded leaves is computed separately. These are energy fluxes per total (senescent plus green) leaf surface area. Therefore, canopy net radiation is computed as the addition of E_a and $R_{n,t}$; and $R_{n,t} = R_{n,t,green} + R_{n,t,senes}$ without the need to further weight by fraction.

Aerodynamic resistances are computed as in SCOPE for the whole mixed canopy, since they depend on meteorology and canopy structure. Consequently water and heat fluxes (H_{green}, H_{senes} and λE_{green}) in senSCOPE are computed with an identical representation of resistances as in SCOPE, but with leaf temperatures differentiated per leaf type. These fluxes are defined per unit of leaf-type surface, and need to be scaled to the fraction of *LAI* represented by each leaf type in the mixed canopy. Eventually, senSCOPE iteratively resolves six temperatures: sunlit and shaded green leaves ($T_{c,u,green}$, $T_{c,h,senes}$), sunlit and shaded senescent leaves ($T_{c,u,senes}$, $T_{c,h,usenes}$), and both sunlit and shaded soil ($T_{s,u}$, $T_{s,h}$).

2.3 Photosynthesis

In senSCOPE, only green leaves photosynthesize and transpire. Photosynthesis is driven by the *PAR* absorbed by chlorophyll ($APAR_{Chl}$; which equals $E_{ap,Chl}$ transformed from W m^{-2} to µmol m^{-2} s^{-1}). The absorbed *PAR* by chlorophyll in green leaves per unit green leaf area is $E_{ap,Chl,green} = E_{ap,Chl} / f_{green}$. Other area-based inputs such as maximum carboxylation rate V_{cmax} [µmol m^{-2} s^{-1}], as well as model outputs (e.g., internal CO_2 concentration, C_i [µmol m^{-3}]) refer to green leaves only. Assimilation (A_c) is therefore initially computed per unit green leaf area. The stomatal conductance (r_{cw}) as output of the leaf biochemical model is further used to calculate the transpiration of green leaves λE_{green}, also per unit green leaf area. Consequently, both fluxes first calculated per unit green leaf area, and later scaled with f_{green}.

2.4 Fluorescence

SCOPE computes leaf level fluorescence emission using three main elements: incident irradiance in the excitation range 400-750 nm, excitation-fluorescence (E-F) matrices ($M(\lambda_e,\lambda_f)$ and $M'(\lambda_e,\lambda_f)$ for backwards and forward fluorescence, respectively), and the amplification factors Φ'_f which are provided by the biochemical model for sunlit and shaded leaves. E-F matrices represent the excitation of chlorophyll and the radiative transfer of incident and re-emitted radiation inside the leaf (Vilfan et al. 2016). In senSCOPE the leaf fluorescence emission is only calculated for green leaves, because for senescent leaves, the E-F matrices equal zero. Then the emission is scaled with f_{green}.

$$E_{\text{l}}^{f} = f_{\text{green}} \cdot \Phi'_f \cdot \left[\left(M'_{\text{green}}(\lambda_e,\lambda_f) + M'_{\text{green}}(\lambda_e,\lambda_f)\right)\right] \otimes E \,, \tag{18}$$

Leaf level fluorescence emission is then propagated to top of the canopy combining the same radiative transfer approach used by SCOPE and the averaged leaf optical properties (ρ and τ) for the mixed canopy.

2.5 Xanthophyll cycle

A recent version of SCOPE incorporates Fluspect-CX (Vilfan et al. 2018), a leaf RTM that simulates the variations in leaf optical properties induced by the activation of the xanthophyll cycle for photosynthetic down-regulation-, and propagates these variations from leaf to canopy level radiances. Changes in leaf optical properties are computed after photosynthesis, as a function of the rate coefficient for non-photochemical quenching (K_{n}) provided by the biochemical module. This rate serves as a scaling factor of leaf ρ and τ between two extreme cases of with completely activated and completely deactivated xanthophyll cycle. In senSCOPE, senescent leaves show no carotenoids, no xanthophyll cycle and no related changes in optical properties; for this reason, the extreme cases calculated on the averaged ρ and τ simulate only variations induced by the green leaves. K_{n} is a rate defining the probability of the different fates of photons exciting chlorophyll, therefore, and similarly to Φ'_f, it does not require additional correction. Therefore, senSCOPE uses the same radiative transfer functions than SCOPE for the propagation of signals related with the xanthophyll cycle.

3. Methods

3.1 Comparison with SCOPE model. Sensitivity analysis

In order to evaluate the differences between senSCOPE and the original model SCOPE (van der Tol et al. 2009), we run two different series of forward simulations modifying separately meteorological variables (F_{meteo}) and vegetation properties (F_{veg}). Eleven different canopies with f_{green} ranging between 0.0 and 1.0 with steps of 0.1 were simulated. As input to SCOPE we used weighted averages of the leaf parameters of each leaf type; similarly as field leaf measurements would be averaged to calculate canopy mean values.

In order to provide realistic meteorological forcing in the simulations F_{meteo}, we used actual measurements acquired in the research site of Majadas de Tiétar between 5th and the 20th May 2016 (day of the year (DoY) 126 and 141, respectively). Fig. 2 summarizes this dataset.

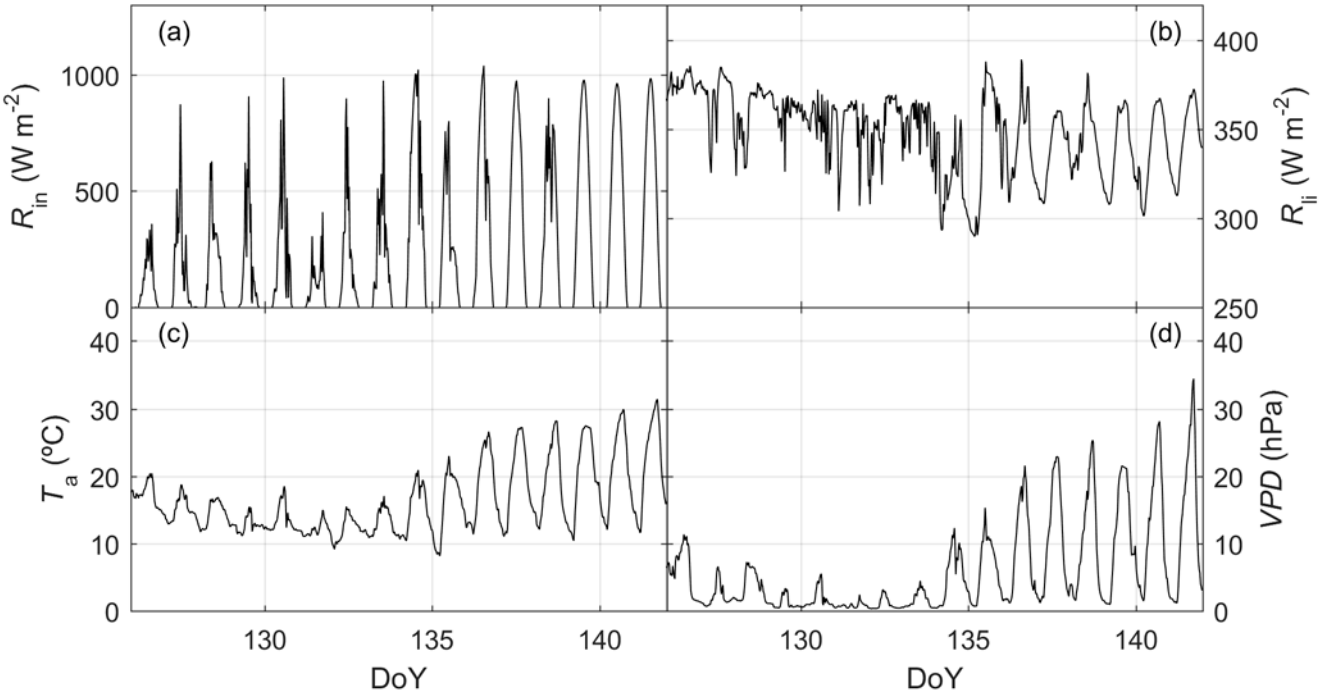

Figure 2. Short wave (a) and long wave incoming radiation (b), air temperature (c) and vapour pressure deficit (d) recorded in Majadas de Tiétar between the 5th and the 20th May 2019 (DoY 126 and 141, respectively) used in the forward simulation F_{meteo}.

Short wave incoming radiation (R_{in}, W m^{-2}), long wave incoming radiation (R_{li}, W m^{-2}), air temperature (T_a, ºC), atmospheric vapour pressure (e_a, hPa), wind speed (u, m s^{-1}), air pressure (p, hPa) and soil moisture (SM_p, % volume) were provided by a sub-canopy eddy covariance station at 1.6 m height (detailed description of the system can be found in El-Madany et al, (2018) and Perez-Priego et al, (2017)). Vapour pressure deficit (VPD, hPa) was calculated from T_a and e_a; also, soil resistance for evaporation from the pore space (r_{ss}, s m^{-1}) was estimated as a function of using SM_p the model SCOPE v1.73. Sun zenith (θ_s) and azimuth (φ_s) angles were computed from timestamps and site location. In the F_{meteo} runs, only the abovementioned variables were modified; leaf and canopy properties were kept constant for the different f_{green} levels tested. Only daytime data (θ_s < 85.0 deg) were used in the simulation; which equals 422 runs per model and f_{green} level.

F_{veg} represented varying vegetation properties under constant meteorological conditions. To do so, we selected midday conditions of the 18th May 2019 (DoY 139). A look up table with 500 samples of C_{ab}, carotenoids concentration (C_{ca}), V_{cmax}, Fluorescence quantum efficiency (f_{qe}), m and LAI was generated using Latin Hypercube Sampling (McKay et al. 1979). C_{ca} and V_{cmax} were constrained as a function of C_{ab} mimicking the relationships (linear function and noise) reported in Sims and Gamon (2002) and Croft et al, (2017), respectively. Table 1 shows the ranges of variation generated for each parameter varying in each F_{veg} simulation. Additionally, a smaller dataset was generated modifying only LAI or C_{ab} (and V_{cmax} and C_{ca} as a function of these) to illustrate an example of the response of models to these parameters. Several model outputs and internal parameters were evaluated. Moreover, we also compared the predicted underlying water use efficiency ($uWUE$, Eq. 19):

$$uWUE = \frac{A}{\lambda E_c}\sqrt{VPD}, \quad (19)$$

where λE_c is the canopy λE, excluding evaporation from the soil.

Table 1. Vegetation parameters used in the forward simulation F_{veg}.

Parameter	Symbol	Units	Range
Leaf chlorophyll content	C_{ab}	µg cm^{-2}	[0.13, 99.98]
Leaf carotenoids content	C_{ca}	µg cm^{-2}	[0.02, 37.26]
Maximum carboxylation capacity	V_{cmax}	mmol m^{-2} s^{-1}	[0.40, 162.78]]
Ball-Berry sensitivity parameter	m	-	[0.05, 39.98]
Fluorescence quantum efficiency	f_{qe}	-	[0.01, 0.03]
Leaf area index	LAI	m^2 m^{-2}	[0.00, 7.99]

The Matlab™ Profiler (Matwoks Inc., Natick, MA, USA) was used to evaluate the computing time and number of calls of the different functions of each model used during these simulations in each run. These metrics, together with the total computation time and the number of unsuccessful runs -where the energy balance does not succeed to converge to a solution-, were used to compare models' performances.

3.2 Comparison with SCOPE model. Forward simulation with observational datasets

SCOPE and senSCOPE were also run forward using observational datasets from the study site of Majadas de Tiétar, Cáceres, Spain (39° 56' 24.68″N, 5° 45' 50.27″W). Observations -and when missing estimates- of vegetation properties and forcing variables integrated at ecosystem scale were used to run both models. Predicted fluxes and reflectance factors where compared with EC observations and hyperspectral airborne imagery.

3.2.1 Study site and datasets

The study site is located in the experimental station of Majadas de Tiétar. It is a managed tree-grass ecosystem combining sparse trees (*Quercus ilex* L. subsp. *ballota* [Desf.] Samp) and a highly diverse herbaceous cover combining numerous species of three main functional plant forms: grasses, forbs and legumes. The climate is continental Mediterranean so that the grassland shows a strong seasonality initiated by greening phase around April, followed by a dry season that starts between May and June, a second re-greening driven by autumn rains, and a dormant phase during winter (El-Madany et al. 2018). The grassland phenology and functioning strongly responds to light and temperature in spring and to water availability in late spring-summer and in autumn (Luo et al. 2018). Several species grow and senesce at different times, usually, in early spring senescent material remnant from the winter is already present, then new material is also generated during spring, where f_{green} can already be already as low as ~0.7 (Melendo-Vega et al. 2018).

In this site, three EC towers monitor three areas of the same ecosystem, one of them fertilized with nitrogen (N) and another one with N plus phosphorous (P), and the control one with no fertilization. These towers include also eddy covariance systems around 15 m above the ground, providing ecosystem-level measurements of carbon and water fluxes. Three sub-canopy towers monitor grassland fluxes ~1.6 m aboveground. Details of the instrumentation and the manipulation can be found in El-Madany et al, (2018) and Perez-Priego et al, (2017). Also, a series of airborne campaigns with the Compact Airborne Spectrographic Imager CASI-1500i (Itres Research Ltd., Calgary, AB, Canada), operated by the Instituto Nacional de Técnica Aeroespacial (INTA) were conducted between 2012 and 2017. From a total of 17 images, a R of the footprint of each EC tower and campaign was extracted. Details of methods and data processing can be found in Pacheco-Labrador et al., (2017). Additionally, in each of the airborne campaigns, destructive sampling of vegetation provided estimates of ecosystem LAI, f_{green}, C_{dm}, C_w, Nitrogen concentration (N_{mass}) and/or C_{ab} and C_{ca}. Further information on protocols and methods can be found in Melendo-Vega et al., (2018), Gonzalez-Cascon et al., (2017) and (Gonzalez-Cascon and Martin 2018).

3.2.2 senSCOPE and SCOPE. Forward simulation and evaluation

Observed/estimated forcing variables and vegetation properties were used to predict fluxes and reflectance factors ±1 day around each flight campaign in each EC tower during daytime. Since no field observations of all the vegetation parameters were available, some of them had to be estimated. When missing, C_{ab} and C_{ca} were estimated from their relationship with N_{mass} observed in the site. Also V_{cmax} was estimated as a function of N_{mass} in the green leaves ($N_{mass,green}$) following the relationship in Feng and Dietze (2013), and assumed 45 μmol m^{-2} s^{-1} for tree leaves. A constant m parameter of 10 was assumed, N and LAD were assumed 1.5 and spherical, respectively. C_s was estimated from the remaining leaf parameters inverting the statistical model described section 3.3.2 and in Appendix A. Soil reflectance was determined by SM_p and the parameters estimated by inversion of the BSM model (Verhoef et al. 2018) in Pacheco-Labrador et al (2019). Also, r_{ss} was estimated as function of SM_p using the model in Pacheco-Labrador et al (2019).

Then, we evaluated the capability of both models to predict GPP, λE, R_n, G, and H comparing SCOPE and senSCOPE predictions with EC fluxes in the site. We also evaluated model performance and structure using predicted fluxes and computing quantities that describe energy partitioning, the evaporative fraction (Eq. 20)

$$EF = \frac{\lambda E}{\lambda E + H}, \quad (20)$$

where λE and H are the total latent heat sensible heat fluxes, respectively.

Emitted irradiance in the TIR (E_t) was compared with net radiometer measurements in the EC towers (CNR4, Kipp and Zonen, Delft, Netherlands); also R were compared with those of the imagery at the time of the overpass.

3.3 Comparison with SCOPE model. Inversion on observational datasets

In order to assess the impact of accounting for senescence material during the estimation of key biophysical (e.g., LAI, C_{ab}) and functional (e.g., V_{cmax}, m) vegetation parameters, we compared the parameter estimates and posterior predictions resulting from the inversion of both models against real

observations in a Mediterranean grassland in the context of a nutrient manipulation experiment with N and P, featuring f_{green} between 0.05-1. In this work, we inverted SCOPE and senSCOPE using the inversion method and approaches proposed in Pacheco-Labrador et al. (2019).

3.3.1 Study site and datasets

The inversion the models is tested using field observations from the understory grass layer of the site of Majadas de Tiétar, Cáceres, Spain, acquired in the context of the Small-scale MANIpulation Experiment (SMANIE) (Perez-Priego et al. 2015). This manipulation nutrient experiment was performed in an open area to minimize the effect of trees. The experimental design consisted of 4 blocks (4 replicates each) with N, P, both (NP) additions, and the control treatment (C, not fertilized). As a result of the fertilization, N, NP and P treatments induced changes in plant community, plant structure and function (Martini et al. 2019; Migliavacca et al. 2017; Perez-Priego et al. 2015). 9 field campaigns took place between 2014-2016 covering spring and early summer. In each block, midday measurements were carried out in two different collars with a dual spectroradiometric system providing hyperspectral *R* and SIF estimates in the O_2-A (F_{760}) and the O_2-B (F_{687}, not in all the campaigns). Diurnal time course of TIR up-welling radiance (L_t) and *GPP* was determined using gas exchange chambers from sunrise to sunset. Fluxes were collected quasi-simultaneously in the same collars of the radiometric measurements at midday. The mismatch between the radiometric and chamber measurements was minimum. Moreover, destructive sampling near by the collars provided estimates of plant traits (f_{green}, *LAI*, and nitrogen concentration N_{mass}). Additional information about instrumentation, sampling methods and data processing can be found elsewhere (Martini et al. 2019; Migliavacca et al. 2017; Pacheco-Labrador et al. 2019; Perez-Priego et al. 2015).

3.2.2 senSCOPE and SCOPE. Inversion and evaluation

We inverted senSCOPE and SCOPE using the same datasets and methodology described for the inversion of SCOPE in Pacheco-Labrador et al. (2019). Observations of *R* and L_t, F_{760} and/or *GPP* were used to estimate *LAI*, C_{ab}, V_{cmax}, *m* and other biophysical parameters (Table 2) using an innovative methodology that combined biophysical and functional constraints in two different steps. Three

458 different sets of constraints (inversion schemes) were tested, each combined in the first step of the
459 inversion (Step#1), noon *R* with noon *GPP* (I_{GPP}), noon *GPP* and F_{760} ($I_{GPP\text{-}SIF}$), or nothing else (I_R).

460 **Table 2. Parameters estimated inverting senSCOPE model**

Parameter	Symbol	Units	Step	Inversion bounds
Leaf chlorophyll content	C_{ab}	µg cm^{-2}	#1	[0, 100]
Leaf carotenoids content	C_{ca}	Mg cm^{-2}	#1	[0, 40]
Senescent material	C_s	-	#1	[0, 7.5]
Leaf water content	C_w,	g cm^{-2}	#1	[6.3·10^{-5}, 0.06]
Leaf dry matter content	C_{dm}	g cm^{-2}	#1	[0.0019, 0.03]
Leaf structural parameter	N	Layers	#1	[1, 3.6]
Leaf area index	LAI	m^2 m^{-2}	#1	[0, 8]
Leaf inclination distribution function	$LIDF_a$	-	#1	[-1, 1]; $\|LIDF_a + LIDF_b\| \leq 1$
Bimodality of the leaf inclination	$LIDF_b$	-	#1	
Maximum carboxylation capacity	V_{cmax}	µmol m^{-2} s^{-1}	#1 & #2	[0, 200]
Ball-Berry sensitivity parameter	m	-	#2	[0, 50]
Fluorescence quantum efficiency	f_{qe}	-	#1 & #2	[0,1]

461

462 In Step#1 biophysical parameters of the SCOPE model and a first guess of V_{cmax} were estimated.
463 Uncertainties were estimated using a Bayesian approach (Omlin and Reichert 1999). Then, in a second
464 step (Step#2) the guess of V_{cmax} was used as a prior and diel cycles of L_t combined with diel *GPP* (I_{GPP}),
465 diel *GPP* and noon F_{760} ($I_{GPP\text{-}SIF}$), or only diel L_t (I_R) were used to estimate the functional parameters
466 V_{cmax} and *m*. f_{qe} was estimated in both steps in the schemes I_{SIF} and $I_{GPP\text{-}SIF}$. Also, pattern-oriented model
467 evaluation was used to assess the results of the different schemes. Unlike the previous work, this time

we increased the inversion bounds (Table 2) for C_{dm} and C_w according to observed distributions in the site (Martín et al. 2019; Melendo-Vega et al. 2018). Also, since previous works found problems to cover the range of R in the near infrared, C_s upper bound was raised up to 7.5 a.u.; a value that allowed covering the low R values found in dry periods in the ecosystem (Martín et al. 2019). The multiple constraint inversion approach proposed in Pacheco-Labrador et al. (2019) provided coherent parameter estimates when *GPP* constrained the inversion (I_{GPP} and $I_{GPP\text{-}SIF}$) using SCOPE; however, uncertainties in part related to the presence of senescent materials biased the estimation some of the parameters, notably C_{ab} during the dry season. In all the cases senescent material also was suspected to induce underestimation of *LAI*.

We used the same methodology to invert senSCOPE on the same datasets in order to compare the results provided by both models and to understand the suitability of using senSCOPE in environments featuring large fractions of senescent leaves. However, in the case of senSCOPE, 6 leaf parameters of two different leaf types must be estimated (Table 2). In order limit the number of free parameters in the inversion, we applied the following constraints: We assumed that green leaves presented no senescent pigments ($C_s = 0$) whereas senescent leaves only presented senescent pigments ($C_{ab} = C_{ca} = 0$). We also assumed that the mesophyll parameter (N) and dry matter content (C_{dm}), were the same for both types of leaves, whereas that water content (C_w) of green leaves was four times higher than senescent C_w (Kidnie et al. 2015). This allowed us reducing the degrees of freedom by 6. We assumed that average leaf parameters (X) could be computed as a linear combination of the parameters of each leaf type (X_{green} and X_{senes}) as in Eq. 21:

$$X = X_{\text{green}} \cdot f_{\text{green}} + X_{\text{senes}} \cdot \left(1 - f_{\text{green}}\right), \quad (21)$$

Given the constrains imposed on leaf parameters, we could directly optimize the leaf averaged parameters in the inversion, similarly as parameters are retrieved in the inversion of SCOPE (Pacheco-Labrador et al. 2019). To do so, X_{green} or X_{senes} are internally calculated solving them from Eq. 21; which is possible in all the cases since at least the value one of them together with f_{green} are known: Either they are equal, 0, or their ratio has been prescribed. senSCOPE includes the additional parameter f_{green}; in order to reduce equifinality and as well as the number of parameters to estimate we prescribed f_{green} by

modelling it as a function of the averaged leaf parameters X using a Neural Network (NN). The NN was trained from a look up table of individual X_{green} and X_{senes} parameters averaged as a function of f_{green}; no assumptions on N, C_w and C_{dm} were made (Appendix A). As a result, the same parameters were estimated in the inversion of SCOPE and senSCOPE.

As in Pacheco-Labrador et al. (2019), we used pattern-oriented model evaluation approach to assess the retrieval of functional parameters, which cannot be determined from individual leaf measurements in the highly biodiverse grassland under study. To do so, we assessed the relationship of V_{cmax} and C_{ab} against N_{mass} in the green fraction of the canopy ($N_{mass,green}$), and in the case of V_{cmax} it was compared with the relationship published by Feng and Dietze (2013) for grasslands. We also evaluated model performance and structure using not directly predicted fluxes, but variables derived from them such as *EF*, which describes energy partitioning (Eq. 19). In addition, a more traditional evaluation was also done assessing the goodness of the fit or prediction of model constraints (R, L_t, F_{760}, and/or *GPP*) and observed parameters (*LAI*, f_{green}).

4. Results

4.1 Comparison of results and performance with SCOPE model: Sensitivity analysis.

For the F_{meteo} runs, green and senescent leaf properties were kept constant for the different combinations of f_{green}. Fig. 3a,b show the leaf optical properties simulated with senSCOPE and SCOPE, respectively. Accordingly Fig. 3c,d shows the TOC Hemispherical-Directional Reflectance Factors (*HDRF*) simulated with each model at midday of DoY 139, the timestamp used for F_{veg} runs. As can be seen, senSCOPE predicts spectroradiometric variables that vary more proportionally to f_{green}, whereas SCOPE simulates stronger absorptions, especially in the visible region. This results from allocating all the absorptive substances to a single leaf type. The largest differences between models are found in the red and blue regions, where senescent leaves in senSCOPE increase scattering. We also verified that when f_{green} equals 1 or 0, the output of both models is the same.

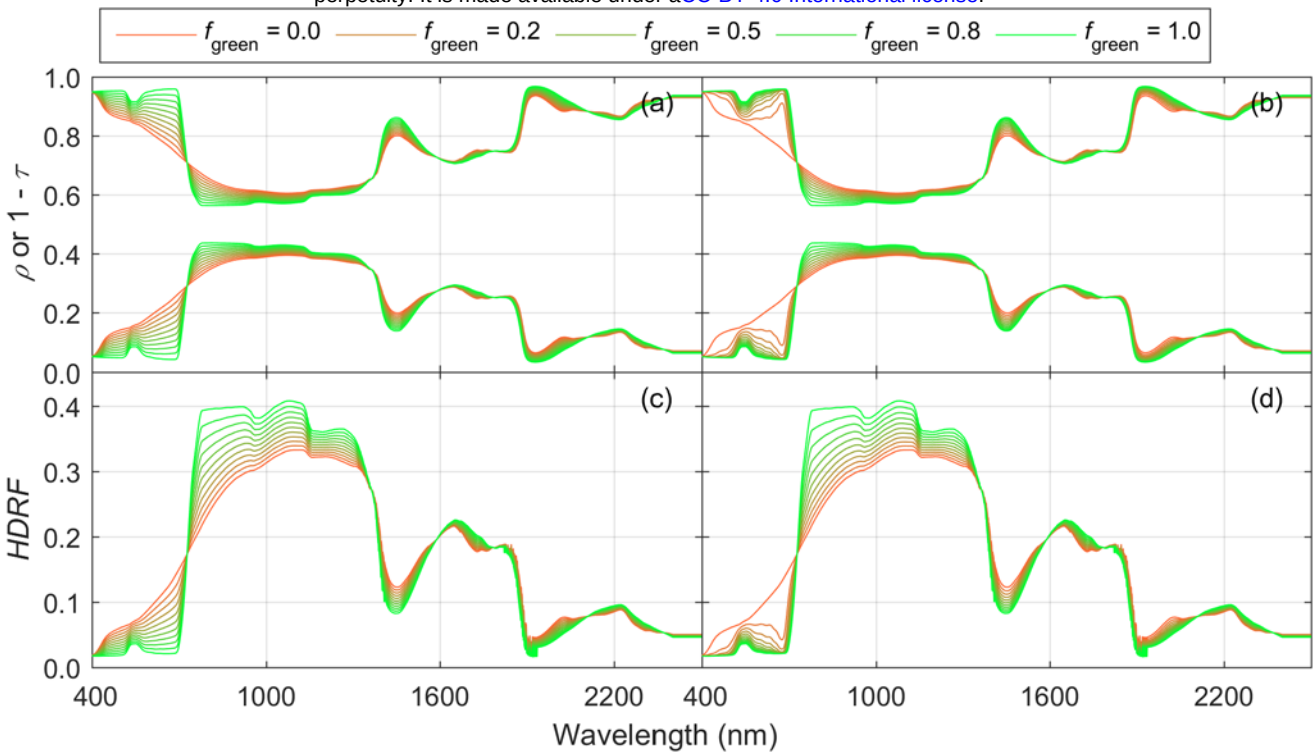

Figure 3. Leaf reflectance and transmittance factors predicted by senSCOPE (a) and SCOPE (b); and top of the canopy Hemispherical Directional Reflectance Factors predicted by senSCOPE (c) and SCOPE (d) for different fractions of green and senescent leaves.

Fig. 4 compares some of the spectoradiometric variables and fluxes predicted by senSCOPE (left semi-columns) and SCOPE (right semi-columns) during DoY 139 in the F_{meteo} runs. As can be seen, those variables that are strongly controlled by radiative transfer in the optical domain ($APAR_{Chl}$ (Fig. 4c,d), the Photochemical Reflectance Index (*PRI*, Gamon et al, (1992)), sensitive to activation of the xanthophyll cycle (Fig. 4q,r) and F_{760} (Fig. 4s,t)) present a stronger and more linear sensitivity to f_{green}. The same is observed for the water and energy fluxes (λE (Fig. 4e,f) and H (Fig. 4g,h)). Differences for variables related with the radiative transfer of thermal radiance seem to be lower (R_n (Fig. 4i,j) and T_c (Fig. 4k,l)). senSCOPE leaves feature a higher absorption of *PAR* per unit green leaf area, which produces a stronger NPQ activation (K_n (Fig. 4m,n)), and a depletion of photosynthetic efficiency around midday (Φ'_f (Fig. 4o,p)) for low f_{green} (unlike the other parameters, these are only representative of green leaves). Notice that the example shown is only representative of the meteorological and

vegetation properties represented during DoY 139, and the differences shown should not be taken generally.

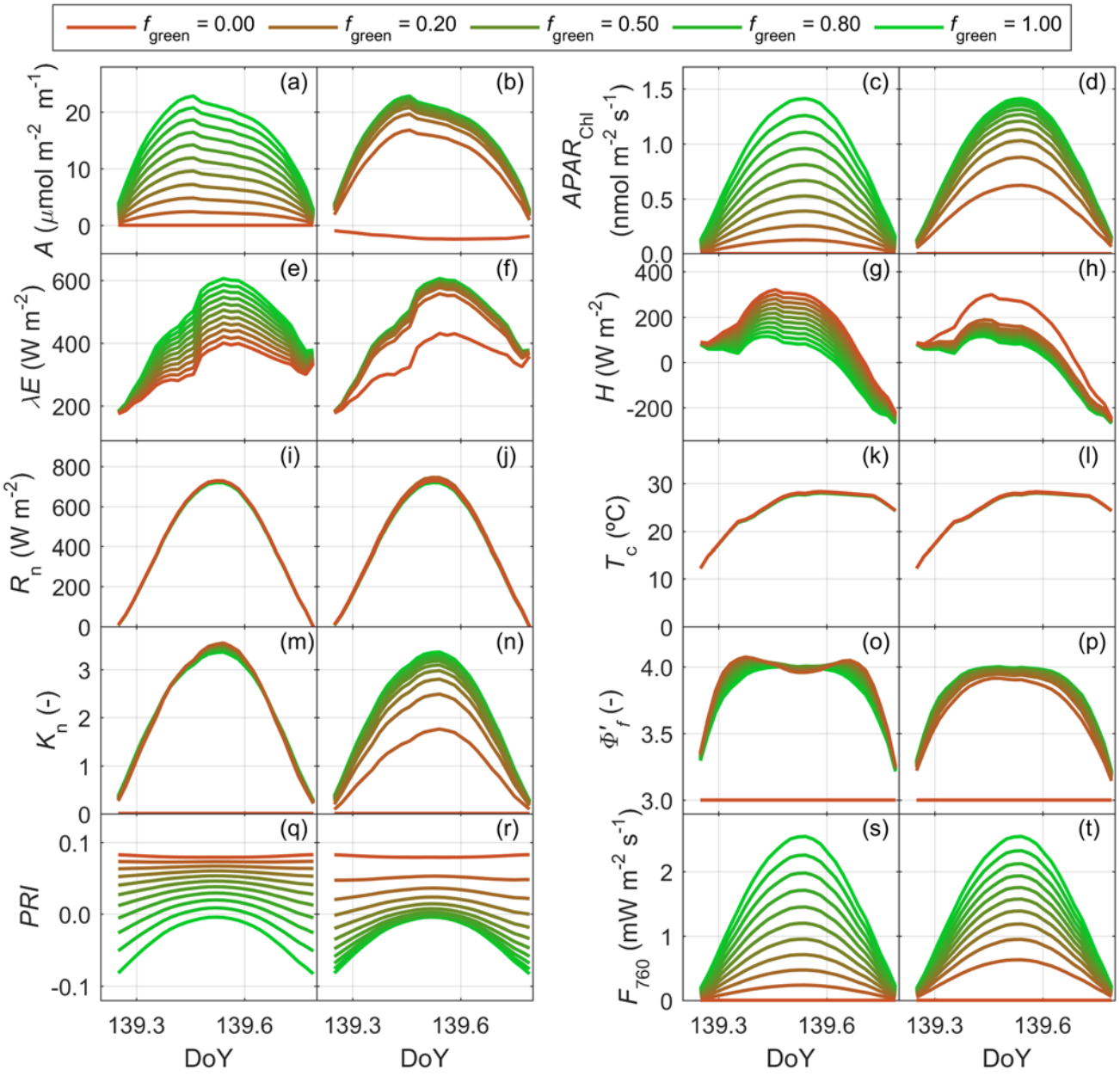

Figure 4. Diel cycles of senSCOPE (left semi-column) and SCOPE (right semi-column) predicted variables on DoY 136: Assimilation (a,b), photosynthetically active radiation absorbed by chlorophylls (c,d), latent (d,e) and sensible heat fluxes (g,h), net radiation (i,j), canopy temperature (k,l), rate coefficient for non-

photochemical quenching (m,n), fluorescence efficiency (o,p), photochemical reflectance index (q,r) and TOC fluorescence radiance at 760 nm (s,t).

Fig. 5 shows the distributions of the difference between fluxes predicted by SCOPE and (minus) senSCOPE for each f_{green} level. Results of the F_{meteo} and the F_{veg} simulations are shown in the left and the right columns, respectively. As can be seen, both under varying meteorological conditions and varying plant properties, the two models predict the same fluxes when $f_{green} = 1$, but not always when $f_{green} = 0$. For $f_{green} < 1$ SCOPE predicts higher assimilation (A, Fig. 5a,b); but in the case of $f_{green} = 0$, where SCOPE predicts negative A due to photorespiration, and senSCOPE represents no photosynthetic leaf area. SCOPE also predicts in most of the cases higher R_n (Fig. 5c,d) and λE (Fig. 5e,f), and lower H (Fig. 5g,h) and G (Fig. 5i,j).

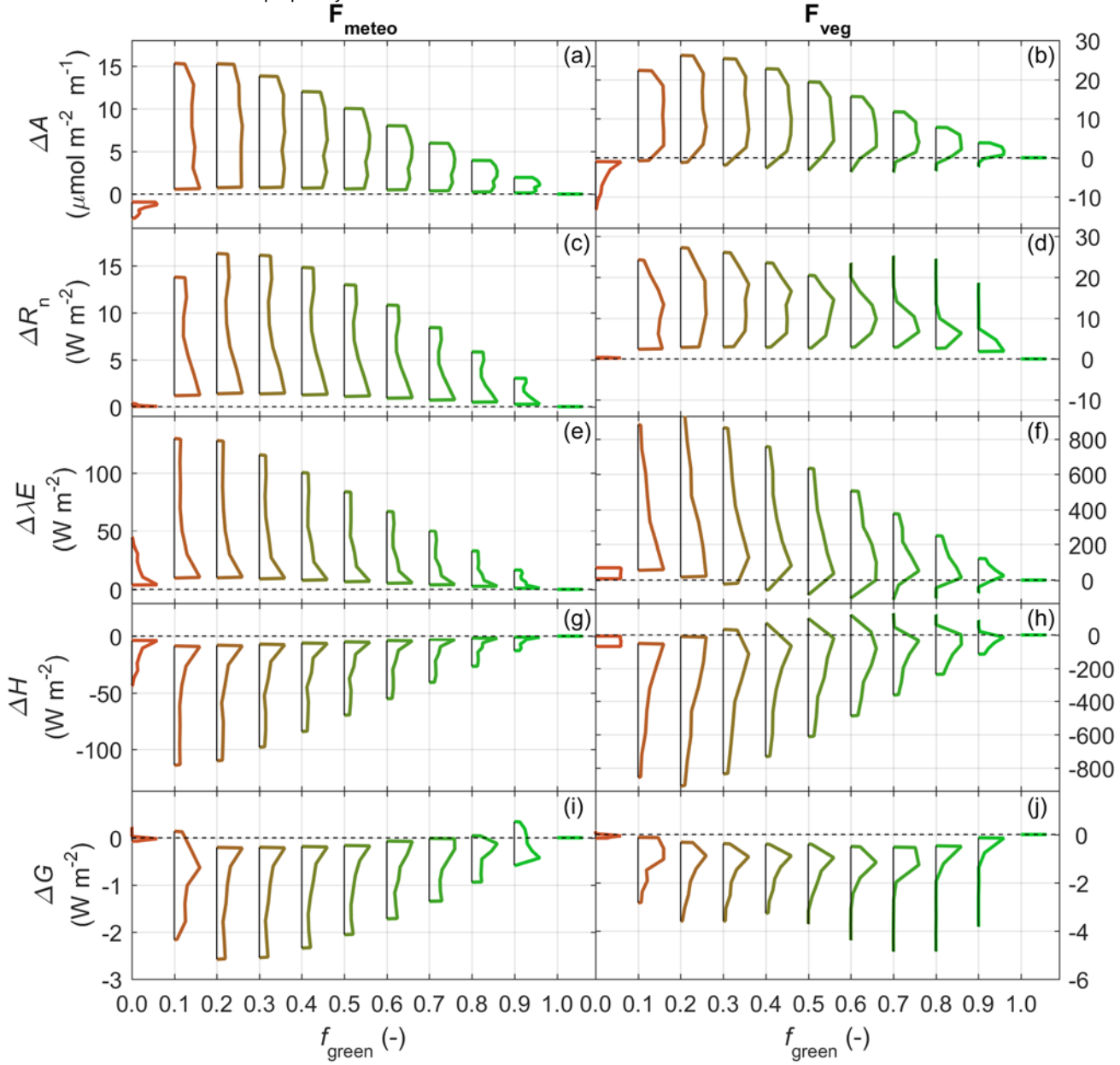

Figure 5. Distributions of the difference between the fluxes simulated with SCOPE and (minus) senSCOPE in the F_{meteo} run (left column) and the F_{veg} run (right column) for different fractions of green leaf area: assimilation (a,b), net radiation (c,d), latent heat flux (e,f), sensible heat flux (g,h) and soil heat flux (i,j).

Differences between predicted fluxes usually maximize when C_{ab} and *LAI* increase (Fig. S1a-e and S2 a-e, respectively). *G* (and R_n) also present large differences for low values of these parameters and mid f_{green}. In the analysis of the forward runs, the differences observed from F_{veg} simulations are often larger than those F_{meteo} simulations since the variability in the meteorological variables is -in relative terms- lower than the variability simulated for the vegetation properties.

For each f_{green} level, Fig. 6 presents the distribution of the difference between variables related to leaf function, as predicted by SCOPE and (minus) senSCOPE. Results of F_{meteo} and F_{veg} are shown on the left and the right columns, respectively. Similar to the fluxes, these variables are integrated according to *LAI* and the probability of each sunlit and shaded leaf angle. $APAR_{Chl}$ (Fig. 6a,b) is equal for both models when the canopy is totally green or senescent. For the rest of the cases SCOPE predicts higher $APAR_{Chl}$, except some cases when $C_{ab} < 10$ μg cm^{-2} (not shown). senSCOPE predicts higher canopy temperature (T_c, Fig. 6c,d) than SCOPE; the largest differences are found when C_{ab} is high (Fig. S1g), or when *LAI* is low (Fig. S2g). Simlarly, *uWUE* (Fig. 6e,f) is higher for senSCOPE, but unlike T_c and most of the variables compared, differences in *uWUE* are more strongly controlled by meteorological conditions than by vegetation parameters. The largest differences in *uWUE* are found under cold conditions with *VPD* < 5 hPa (not shown). senSCOPE presents also higher K_n (Fig. 6g,h). Differences between models predictions increase with *LAI* (Fig. S2i), and decrease with C_{ab} (Fig. S1i). Φ'_f (Fig. 5i,j) is most often higher for senSCOPE than for SCOPE, especially if *LAI* is high and C_{ab} is low (not shown). On the other hand, SCOPE predicts higher Φ'_f when *LAI* is low (Fig. S2j) or when C_{ab} is low and *LAI* is moderate (Fig. S1j). As expected, both models predict the same values for these variables when $f_{green} = 1$.

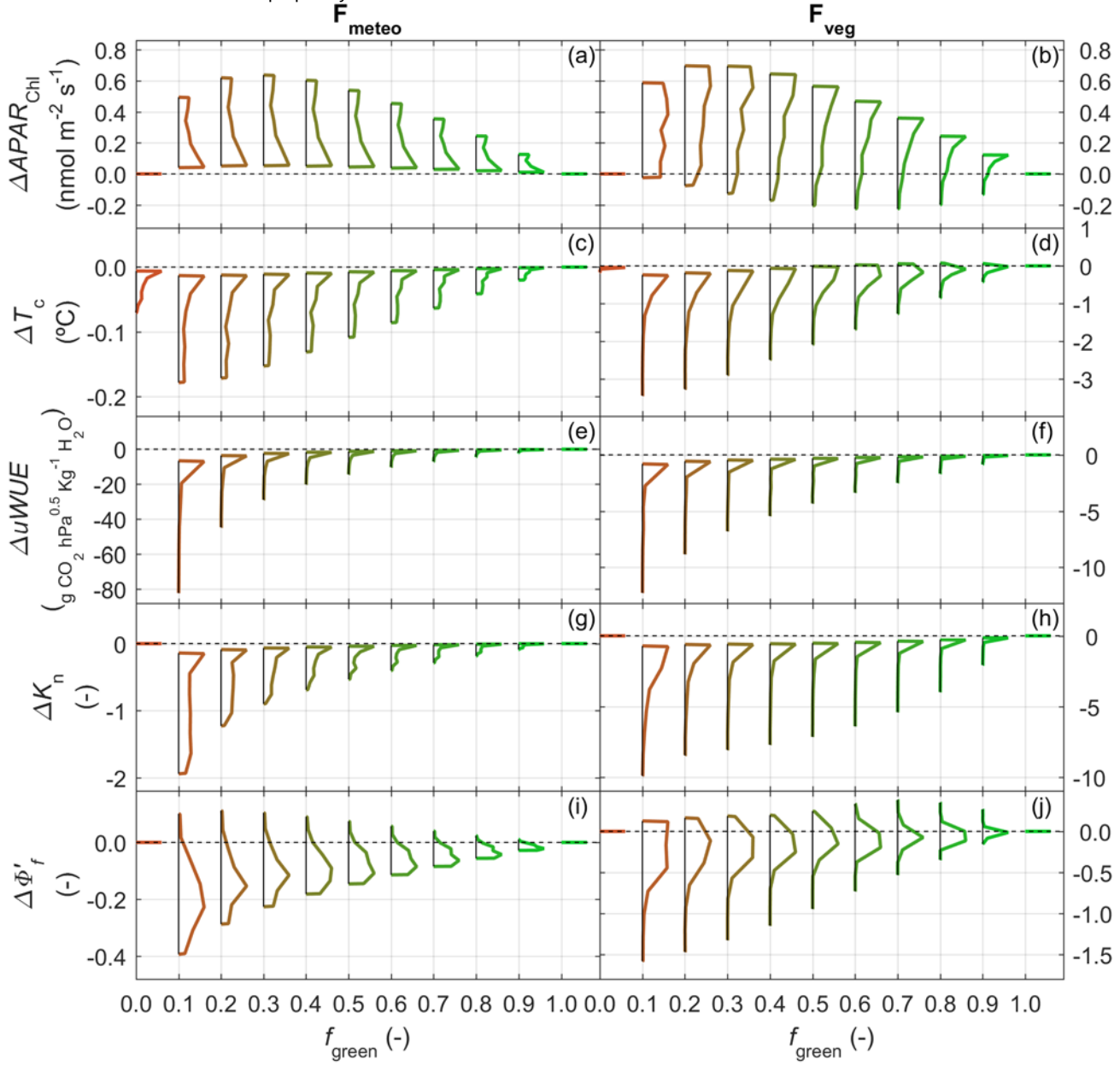

Figure 6. Distributions of the difference between variables indicative of plant physiology simulated with SCOPE and (minus) senSCOPE in the F_{meteo} run (left column) and the F_{veg} run (right column) for different fractions of green leaf area: photosynthetically active radiation absorbed by chlorophylls (a,b), canopy temperature (c,d), underlying water use efficiency (e,f), rate coefficient for non-photochemical quenching (g,h) and fluorescence efficiency (i,j).

Fig. 7 shows the distribution of some TOC spectroradiometric variables predicted by SCOPE and (minus) senSCOPE for each f_{green} level. Results of the F_{meteo} and the F_{veg} simulations are presented in the left and the right columns, respectively. F_{687} (Fig. 7a,b) and F_{760} (Fig. 7c,d) are larger for SCOPE in most of the cases the cases; the largest differences are found for low f_{green} and large C_{ab} (Fig. S1k,l) and LAI (Fig. S2k,l). Differences in *PRI* are negative for Fmeteo, but of both signs for Fveg (Fig. 7e,f). In this case, the influence of vegetation parameters is more complex and less linear than in other variables; since it depends on the combination of C_{ab} and C_{ca}, their ratio and *LAI* (not shown). A similar analysis carried out on the *PRI* computed from reflectance factors where the effect of the xanthophyll cycle is not simulated reveals that differences between models rather respond to biophysical properties than to differences in function (not shown). Two more spectral indices responsive to pigments content and canopy structure are also analysed. Fig. 7g,h presents the differences for the Normalized Difference Vegetation Index (*NDVI*, Rouse et al, (1974)); Fig. 7i,j present differences for the MERIS Terrestrial Chlorophyll Index (*MTCI*, Dash and Curran (2007)); senSCOPE predicts lower and higher values, respectively. For these indices, the absolute difference between models increase as f_{green} decreases, and as C_{ab} and *LAI* increase (Fig. S1n,o and S2n,o, respectively).

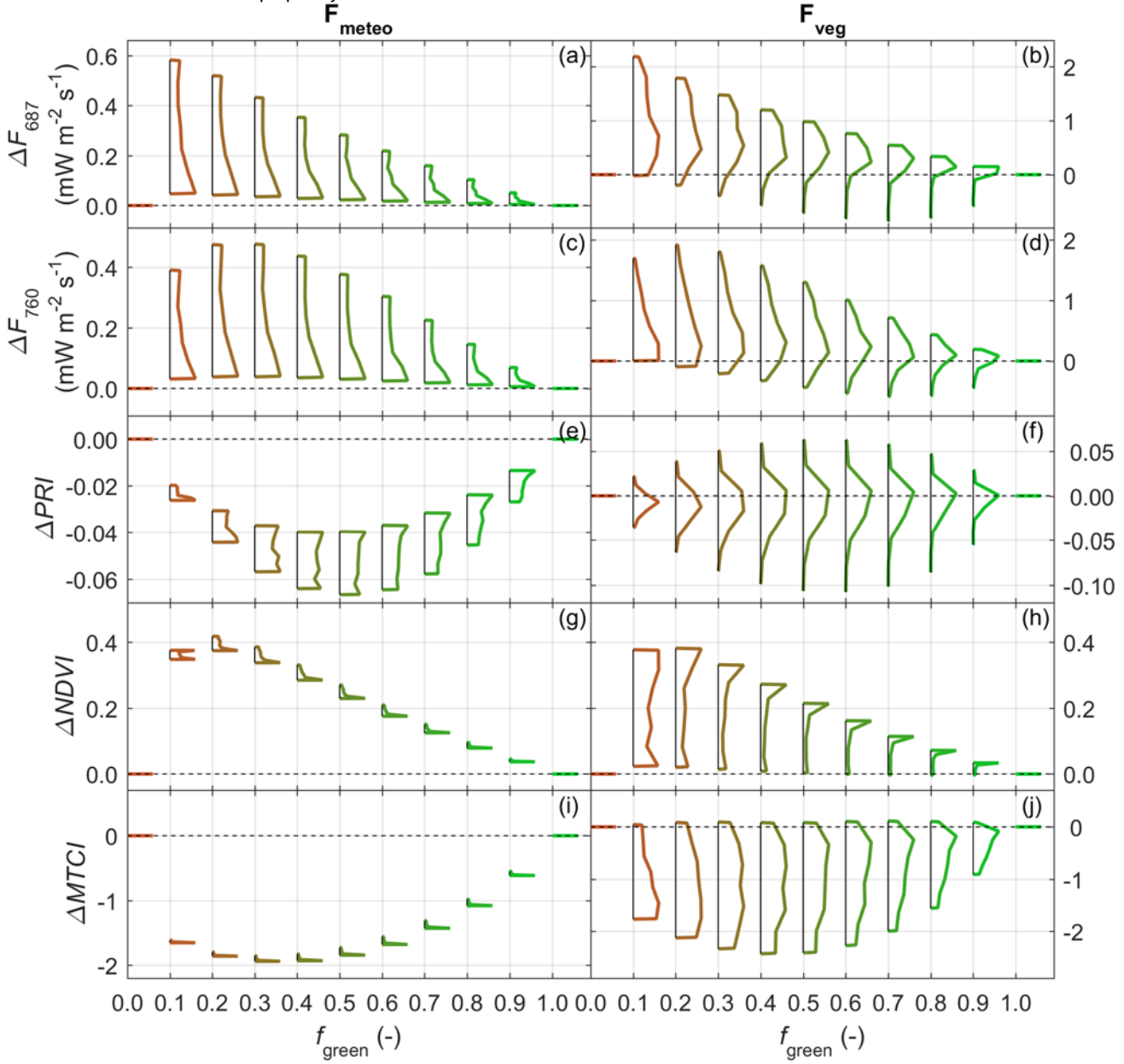

Figure 7. Distributions of the difference between spectral variables indicative of plant physiology, structure and biochemical composition simulated with SCOPE and senSCOPE in the F_{meteo} run (left column) and the F_{veg} run (right column) for different fractions of green leaf area: TOC fluorescence radiance at 687 nm (a,b), TOC fluorescence radiance at 760 nm (c,d), photochemical reflectance index including effects of xanthophyll cycle (e,f), normalized difference vegetation index (g,h) MERIS terrestrial chlorophyll index (i,j).

4.2 Comparison with SCOPE model. Forward simulation with observational datasets

Fig. 8 compares the different variables predicted by SCOPE and senSCOPE vs. the fluxes measured by the EC towers and *R* acquired by the airborne hyperspectral imager in the site of Majadas de Tiétar. The comparison is done using Total Least Squares (Golub and Loan 1980). In general, senSCOPE achieves higher coefficients of determination (R^2) n lower relative root mean squared errors (*RRMSE*). Both models overestimate high *R* (Fig. 8a), and *GPP* (Fig. 8b); but senSCOPE is less deviated. SCOPE overestimates λE and *EF*, and underestimates *H* more than senSCOPE. Both models predict R_n quite accurately and precisely; but senSCOPE predicts R_n, E_t and *G* with slightly larger errors and in some cases lower R^2 than SCOPE.

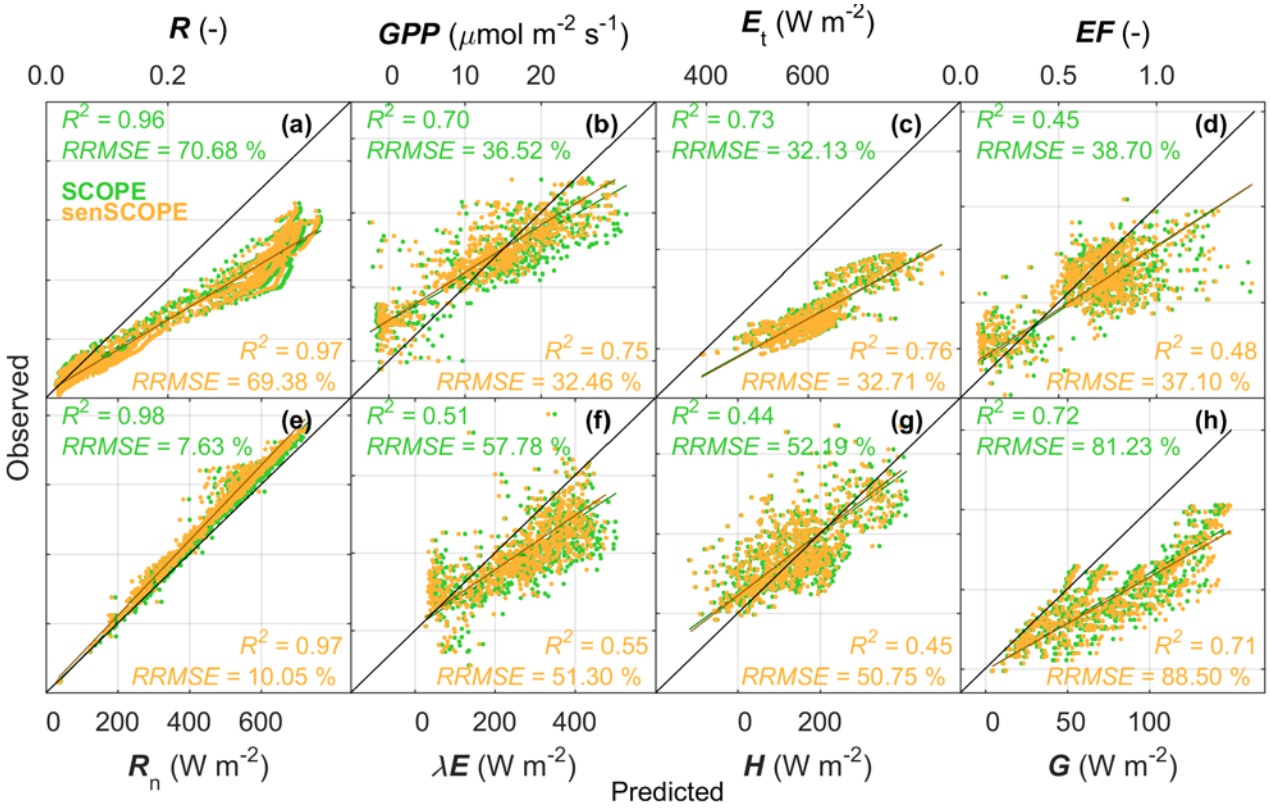

Figure 8. Comparison of observed and predicted fluxes and reflectance factors at ecosystem scale. Predictions are done by SCOPE (green) and senSCOPE (orange) using field observations or estimates of vegetation properties, as well as forcing variables measured at the research station of Majadas de Tiétar ±1 day around different airborne campaigns.

4.3 Comparison with SCOPE model. Inversion on observational datasets

Fig. 9 summarizes the capability of SCOPE and senSCOPE to fit/predict the variables used as inversion constraints in the different schemes tested; notice that not all the constraints are used to optimize parameters in all the schemes. The relative differences between the statistics of the fit are calculated as $(100 \cdot (x_{senSCOPE} - x_{SCOPE})/ x_{SCOPE})$; where x is the statistic and the respective model is presented in the subscript. R^2 is estimated using Total Least Squares (Golub and Loan 1980), and the relative root mean squared error (*RRMSE*) and mean average error (MAE) result of the comparison of the observed/predicted values. Posterior uncertainty (σ_{post}) is estimated according to Omlin and Reichter (1999). The relative differences of R in the visible spectral region (R_{Vis}, Fig. 9a-d) and the near infrared (R_{NIR}, Fig. 9e-h), *GPP* (Fig. 9i-l), F_{760} (Fig. 9m-p) and L_t (Fig. 9q-t) are presented for the three different inversion schemes tested. R is used in all the inversion schemes. senSCOPE fits R_{Vis} and R_{NIR} more poorly than SCOPE in the schemes I_{GPP} and $I_{GPP\text{-}SIF}$; whereas in the case of I_R senSCOPE these are better fit and posterior uncertainties are lower than for SCOPE. senSCOPE slightly improves the fit of *GPP* when this is a constraint of the inversion; however, σ_{post} almost duplicate (values ~80%, out of the plot scale). As in Pacheco-Labrador et al., (2019) I_R fails to accurately fit *GPP*, but σ_{post} is lower for senSCOPE. senSCOPE fit of F_{760} improves respect to SCOPE when this is a constraint of the inversion ($I_{GPP\text{-}SIF}$), but σ_{post} increase in all the cases. senSCOPE fits L_t more poorly than SCOPE, but σ_{post} decrease in all the cases.

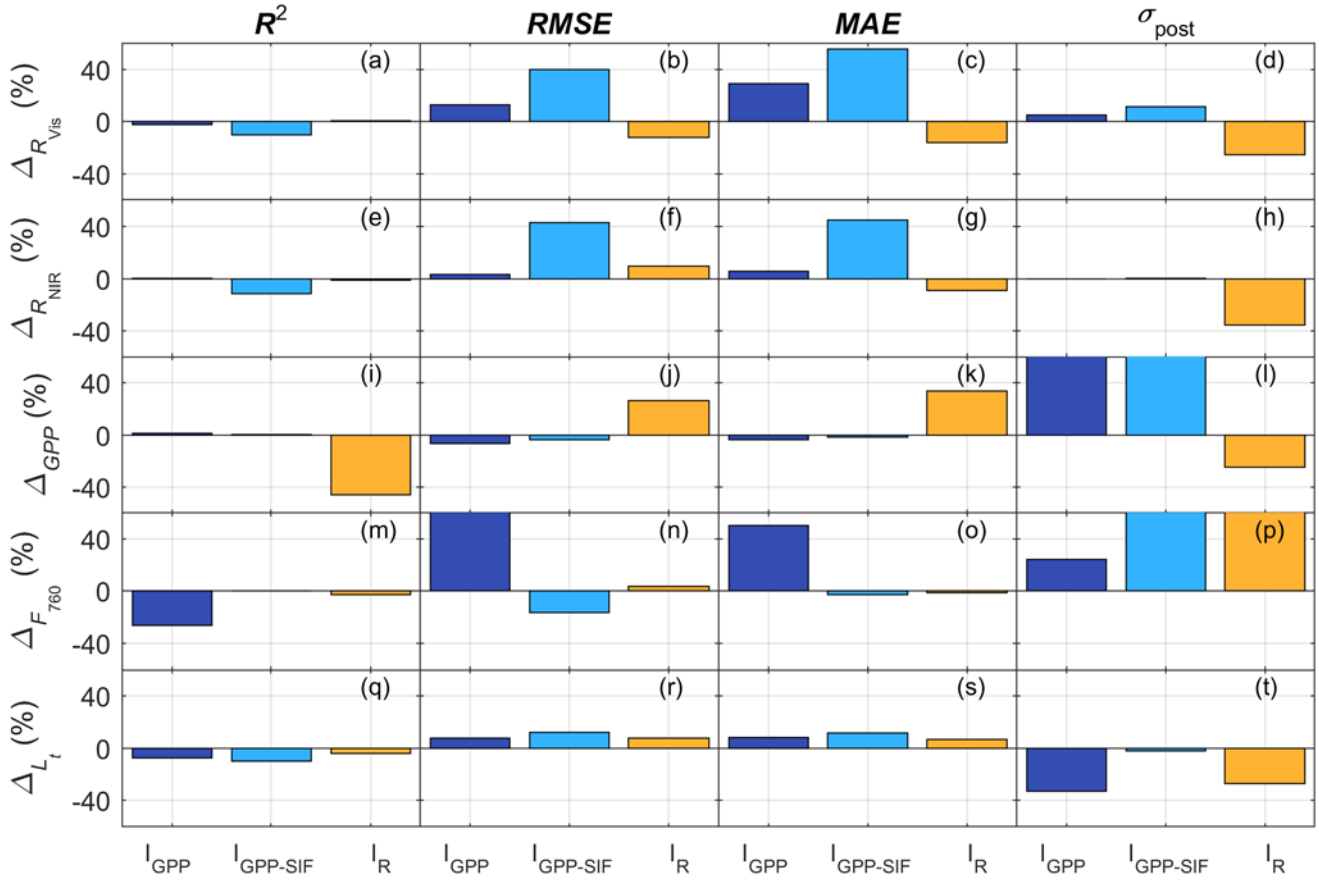

Figure 9. Relative difference between the fit/prediction statistics of the inversion constraints obtained by senSCOPE and SCOPE for the different inversion schemes.

Fig. 10 compares the most relevant model parameters estimated by SCOPE and senSCOPE for the different inversion schemes tested (presented by columns, from left to right: I_{GPP}, $I_{GPP\text{-}SIF}$, I_R). Parameters are evaluated both using field observations and pattern-oriented model evaluation approach. *LAI* (Fig. 10a-c) and f_{green} (Fig. 10d-f) are compared against observations using Total Least Squares (Golub and Loan 1980). As can be seen, senSCOPE predicts similar *LAI* values but show higher R^2 and significance. senSCOPE is also capable of providing reasonable estimates of f_{green}, these are often overestimated but still within the bounds of the relationship C_{ab}-f_{green} observed in the site (Fig. S3). $N_{mass,green}$ is used to evaluate V_{cmax} (Fig. 10g-i) and to compare the relationship between both variables with the one reported in the literature for grasslands (Feng and Dietze 2013). Notice that senSCOPE

651 V_{cmax} is provided per unit green leaf area and is thus comparable with SCOPE estimates and the
652 literature data. Results are coherent with those presented in Pacheco-Labrador et al., (2019), I_R fails to
653 constrain V_{cmax}, whereas the schemes using *GPP* provide relationships with $N_{mass,green}$ which are closer
654 to those in the literature. V_{cmax} estimates are very similar for both models in I_{GPP}; however, the use of
655 F_{760} in $I_{GPP\text{-}SIF}$ seems to slightly deviate the adjusted logarithmic model from the one fit to the data in
656 Feng and Dietze (2013). Similarly, C_{ab} (per total leaf area) is evaluated against N_{mass} of the whole
657 canopy (Fig. 10j-l), and their relationship is compared with field observations of both variables in the
658 site of Majadas de Tiétar. When *GPP* constrains the inversion senSCOPE and SCOPE estimates are
659 similar and follow the relationship observed in the field. However, as in Pacheco-Labrador et al.,
660 (2019), SCOPE I_{GPP} and $I_{GPP\text{-}SIF}$ estimates present high values during the dry period, which stand out of
661 the relationship with N_{mass} between 0.5-1.3 %. senSCOPE corrects most of these values, especially in
662 the scheme I_{GPP}; while the scheme $I_{GPP\text{-}SIF}$ still preserves some of these high values. Fig. 10m-o
663 compares predicted and observed *EF* using Total Least Squares (Golub and Loan 1980). In general,
664 both models achieve similar results when *GPP* constrains the inversion; however, senSCOPE R^2 are
665 lower than in SCOPE. As in Pacheco-Labrador et al., (2019), I_R fails to constrain functional parameters.

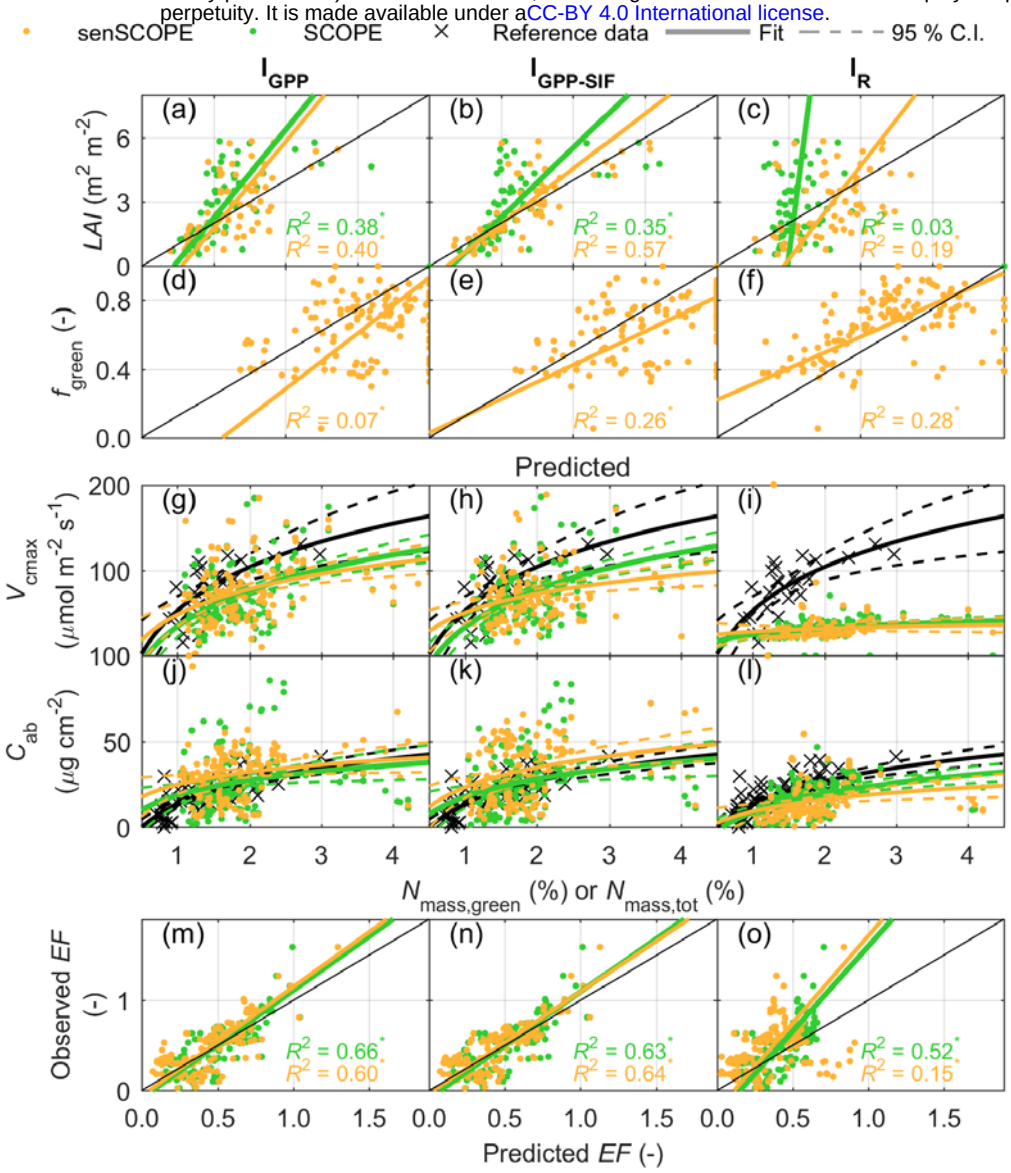

666

667 **Figure 10. Summary of the parameters' evaluation using observations and pattern-oriented model**
668 **evaluation for the four inversion schemes tested. Leaf area index, (a-c) and green fraction of leaf surface**
669 **(d-f), and evaporative fraction (q-t) are compared with field observation using Total Least Squares (Golub**
670 **and Loan 1980). Significance is described with the symbols $^{\cdot}$ for *p*-values $0.05 \leq p < 0.10$; and * for $p < 0.05$.**
671 **The 1:1 line is shown in black. Maximum carboxylation rate (g-i) and chlorophyll concentration (j-p) are**
672 **evaluated against nitrogen content in green leaves and total nitrogen content, respectively and compared**
673 **with data from the literature (Feng and Dietze 2013) the first, and relationships observed in the field, the**
674 **second A logarithmic relationship is fit in both cases, the 95 % confidence interval is show with dashed**
675 **lines.**

5. Discussion

This manuscript describes and evaluates senSCOPE, a version of the model SCOPE representing separately radiative transfer and physiological processes of green and senescent leaves; which is relevant in canopies featuring important senescent leaf area fractions. senSCOPE is evaluated against SCOPE 1) by direct comparison of forward synthetic simulations, 2) by comparison of simulated and observed ecosystem-scale fluxes and reflectance factors, and 3) by evaluation of parameter estimates and predicted variables via inversion of the models against a comprehensive dataset including hyperspectral optical *R*, as well as *GPP*, SIF and TIR radiance. These data were collected in a fertilization experiment with varying nitrogen and phosphorous additions and degrees of water stress. Results show that in senescent canopies senSCOPE improves the forward modelling of radiative transfer, photosynthesis and fluxes; and that in inversion -if suitably constrained-, it improves the estimation of C_{ab}. At the same time, the performance of both models is comparable when green leaves dominate.

senSCOPE distributes senescent and remaining pigments in two conceptual leaves (green and senescent) and predicts separately their respective optical properties, which are later combined. This approach was already proposed by Bach et al., (2001) and used in later works (Bach and Verhoef 2003; Houborg et al. 2009; Houborg et al. 2015; Houborg and McCabe 2016; Verhoef and Bach 2003). This dual-leaf approach generates averaged "brighter" leaves since not all the absorbent species are located in the same leaf (Fig. 3). This has relevant consequences for the canopy-RTM, especially in those spectral regions where senescent and the rest of the pigments overlap, and therefore for $APAR_{Chl}$. senSCOPE produces reflectance factors and $APAR_{Chl}$ that close-to-linearly vary with f_{green}; whereas in the case of SCOPE, these variables vary logarithmically with f_{green} since leaves absorptivity saturate due to the large presence of pigments. This saturation, combined with the fact that R_{NIR} was overestimated during senescence, led to unrealistically high C_{ab} estimates during the dry period when a strong functional constraint –*GPP*– was used (Pacheco-Labrador et al. 2019). Notice that only the constraint *GPP* provided robust estimates of functional parameters. In the present work, we repeated the inversion of SCOPE allowing higher C_s than in Pacheco-Labrador (2019) since this allowed predicting low R_{NIR}

values observed in the site (Martín et al. 2019). This approach improved the fit of R_{NIR} for all inversion schemes during SCOPE inversion (not shown), but did not solve the overestimation of C_{ab} in the most strongly constrained schemes (I_{GPP} and $I_{GPP\text{-}SIF}$, Fig. 10a,b). senSCOPE fitted less precisely the inversion constraints, and in some cases posterior uncertainties increased due to the strong control that f_{green} has on most of the model outputs (Fig. 9). For I_R senSCOPE improved the fit of *R*, but the opposite occurred when *aPAR* was constrained by *GPP*, suggesting that the model might not still represent accurately the observed grassland However, senSCOPE led to C_{ab} values more soundly related with N_{mass} than SCOPE during the dry season (schemes I_{GPP} and $I_{GPP\text{-}SIF,}$ Fig. 10j,k).

The fact that senSCOPE limits photosynthesis and transpiration to the green fraction results in a close-to-linear relation between f_{green} on the one hand, and *A* and λE on the other hand (Fig. 4 and 5). SCOPE predicts higher assimilation and transpiration unless f_{green} is very low (~0); in that case *A* is negative while λE is still high. Contrarily, R_n and *G* predictions are similar for both models; also, differences in *H* are lower than for λE, but still in senSCOPE *H* varies more linearly with f_{green} than in SCOPE (notice that f_{green} is not a SCOPE parameter, but is used to average leaf parameters). In the forward simulation at ecosystem scale senSCOPE predicted most of the ecosystem fluxes better than SCOPE (Fig. 8). In this case we assumed a fixed value for *m*, which might be not completely realistic; however additional works at ecosystem scale have shown that senSCOPE can more robustly represent water use efficiency than SCOPE (not shown). In the inversion at plot level, senSCOPE predicted *GPP* better than SCOPE when used as constraint (Fig. 9k-o). In contrast, *EF* was predicted more poorly in all the schemes. senSCOPE assumes no transpiration from senescent leaves; however evaporation from their surface might be relevant when these are moisturized by dew or rainfall. Neither SCOPE nor senSCOPE represent that process and their use after such situations might result uncertain.

In inversion, both SCOPE and senSCOPE underestimated *LAI*, while senSCOPE overestimated f_{green} (Fig. 10a-h). As discussed in Pacheco-Labrador et al, (2019) and Melendo-Vega (2018), the optical properties of dry standing material might not be accurately described by RTM, leading to an overestimation of $R_{NIR,}$ which seems to be counter-weighted in inversion by reducing *LAI*. In fact, inversion schemes using *GPP* (I_{GGP} and $I_{GPP\text{-}SIF}$) improved the estimation of *LAI* since *GPP* demands

higher $APAR_{Chl}$ in exchange for increasing the fitting error of R_{NIR} (Pacheco-Labrador et al., (2019), this work). In senSCOPE, underestimation of *LAI* was also compensated also by overestimating f_{green}. These facts suggest that the optical properties of the senescent material and/or the death standing material of this grassland (and likely other ecosystems) are not accurately represented, leading to biased estimates of some of the parameters. In fact, it was necessary increasing the upper bound of C_s to be able to predict low R_{NIR} in the dry season. We allowed C_s up to 7.5; whereas values up to 5.0 are reported in literature (Houborg and Anderson 2009). Too high C_s might have led to unrealistic representation of ρ and τ of senescent leaves, very dark in the visible region but also with low R_{NIR}. In some cases SCOPE estimated C_s = 7.5, whereas senSCOPE predicted C_s < 5 in most of the cases (Fig. S4c). Apart from *LAI*, C_{dm} and C_w, -which are weakly constrained because the spectroradiometric measurements did not include the short wave infrared range (SWIR)-, might have been affected by this problem. SCOPE and senSCOPE estimates of C_{dm} often hit the upper bound stablished from observations in the field. High C_{dm} also serves to reduce R_{NIR}. In contrast, senSCOPE C_w estimates are less often saturated; C_w has little effect below 970 nm, but influences leaf optical properties in the SWIR. The relationship between *N*, C_{dm} and C_w of green and senescent leaves assumed during inversion might have contributed to increase the uncertainty of the parameter estimates; for example, it has been observed that leaf thickness decreases during senescence (Castro and Sanchez-Azofeifa 2008); whereas other works assign high N values to senescent leaves (Houborg et al. 2009). However, a balance between model error and equifinality must be also observed. Site-specific relationships between the parameters of each leaf type or relationships found in global databases could be used in the future to improve the representation of semi-arid canopies. senSCOPE does not include improved calibrated absorption coefficients or refractive indices to more realistically represent senescent leaves and death standing material, but it offers a formally more correct representation of mixed canopies. The model improves the representation of these canopies, which could be used in the future to calibrate or validate specific absorption spectra of senescent material. senSCOPE can also be applied to other canopies, such as crops and forests, which are characterized a senescent stage. Moreover, the approach adopted in senSCOPE could be similarly used to represent other mixed canopies combining plants with different biophysical properties and function, such as C3 and C4 species. An additional problem for the representation of mixed canopies

would be the vertical distribution of the senescent material. The impact on the observed R and fluxes is unclear, and further research is needed in this direction. In such studies, senSCOPE could also be extended to other versions of SCOPE, such as mSCOPE (Yang et al. 2017) to describe the vertical distribution of senescent matter.

f_{green} is a critical parameter in senSCOPE, it strongly controls RTM and fluxes and increases equifinality of the inverse problem. Thus, the use of prior information about is this variable is strongly recommended during inversion. For this reason, in this work f_{green} was indirectly predicted from leaf parameter estimates using a NN while the model was inverted. The design of this model was critical to achieve acceptable results, and during training C_{ab} (and C_{ca}) had to be limited to the ranges observed in the study site (up to ~40 µg cm^{-2}). During inversion higher C_{ab} values were allowed, but still, C_{ab}-f_{green} estimates stood within or very close to the bounds observed and used to train the NN (Fig. S3)

As a result of the combination of changes in RTM and photosynthesis, not only carbon and water fluxes, but also photosynthetic efficiency and downregulation resulted modified (Fig. 6). On one side, senSCOPE tends to predict higher canopy temperatures than SCOPE, especially when f_{green} decreases. Senescent leaves are warmer than green leaves, but senSCOPE green leaves are not necessarily cooler than SCOPE leaves (not shown). Leaf temperature strongly influences photosynthetic efficiency and together with $APAR_{Chl}$ on photosynthesis down-regulation. Fig. 4m,h show how senSCOPE diel cycles of K_n reach higher midday values than SCOPE. SCOPE predicts larger variability of K_n as a function of f_{green} under conditions of low illumination, whereas senSCOPE K_n varies more strongly with f_{green} under high temperature and irradiance conditions (not shown). Non-photochemical quenching has also different effects on the predicted Φ'_f. For example, Fig. 4o,p show how senSCOPE predicts a decrease of this efficiency at midday whereas this is hardly noticeable for SCOPE. K_n and Φ'_f are fundamental variables to mechanistically interpret SIF signals to determine functional status of vegetation and stress (Frankenberg and Berry 2018; Porcar-Castell et al. 2014). Thus considering the differences shown, both models can lead to very different interpretations. Adequate representation of physiological processes and their drivers is fundamental to mechanistically interpret these signals; but also the representation of the spectral variables used to obtain information about these processes, such as fluorescence radiance or

PRI. Similarly as *R*, spectral indices vary more linearly with f_{green} in senSCOPE than in SCOPE (e.g., Fig. 4q,r). Unlike other spectroradiometric variables, *PRI* show no clear differences between models (e.g. distributions of the difference centre around 0). PRI is known to result sensitive to pigments pool, ratio and to *LAI* (Gamon and Berry 2012; Garbulsky et al. 2011); results of this work also show that this index is also strongly sensitive to the presence of senescent material. The magnitude of SIF emissions is also modified by senSCOPE, which tends to predict less SIF when f_{green} decreases, (Fig. 7a-d).

In this study we compare the inversion of SCOPE and senSCOPE using the data and approaches of in Pacheco-Labrador et al, (2019), but allowing for higher values for C_s (as well as C_{dm} and C_w). The wider parameter bounds did not change significantly the results obtained with SCOPE, and differences were mainly related to the use of senSCOPE; which improved the estimation of C_{ab} in the dry season. As with SCOPE, SIF (not shown) and *R* failed to constrain functional parameters (e.g., V_{cmax}) and *LAI*; and only inversion schemes relying on *GPP* provided robust estimates. However with senSCOPE, the schemes relying on SIF reduced their performance respect to SCOPE. $I_{GPP\text{-}SIF}$ fitted the inversion constraints more poorly, and could not correct high C_{ab} estimates during senescence as much as I_{GPP}. This might be result from the use of large C_s, which suggests further work is needed to more accurately characterize the optical properties of death standing and senescent material. Also for senSCOPE, functional parameters resulted insensitive to I_R constraints (partly due to inversion method, see Pacheco-Labrador et al, (2019)). Bayat et al., (2018) inverted SCOPE using *R* and found troubles to predict low *GPP* and λE in a grassland during senescence, which was corrected constraining the model with *R* and TIR radiance to reduce V_{cmax} during this period. Fig. 10i-l compares V_{cmax} estimates of both models; for senSCOPE V_{cmax} is presented respect to green leaf area, whereas in SCOPE, it is presented respect to total leaf area (all considered "green"). As can be seen, when adequately constrained estimates of both models are comparable. In senSCOPE *GPP* scales with f_{green}, and V_{cmax} (in the green leaves) does not need to decrease to predict low assimilation.

senSCOPE is computationally more demanding (around 10% slower) than SCOPE since more processes and calculations are needed, and more iterations are required to close the energy balance (Table S5). However, senSCOPE seems more robust and provides lower energy balance closure error.

Since performance of both models is similar for large f_{green}, both models can be alternately used through the season according the presence of senescent material.

6. Conclusions

The combination of advanced radiative transfer models with models representing exchanges of matter and energy between vegetation, soil and atmosphere is bringing new opportunities to improve our understanding of ecosystem function from remote observations. For example, the model SCOPE is being used in the last years with this purpose. However, the accuracy with which these models represent reality limits their application; and ecosystem-specific features can bias results and their interpretation. In this context, we present the model senSCOPE; which adapts SCOPE radiative transfer, energy balance, photosynthesis and transpiration in homogeneous canopies with mixed green and dry leaves. The separated representation of green and senescent leaves significantly modifies the simulation of fluxes and spectra signals respect to a model featuring a single leaf with "averaged" properties. senSCOPE reflectance factors, carbon assimilation and water and energy fluxes linearly scale with f_{green}; it also improves the prediction of these variables in forward simulations as well as the estimation of vegetation parameters, notably C_{ab}, during the dry season. This is significant for the remote sensing of vegetation function of semi-arid ecosystems, and potentially for phenology monitoring. Despite the improvements, results suggest that not only model structure needs to be corrected; a more accurate characterization of the optical properties of senescent material in grasslands is still needed. The use of SCOPE and derived models is growing in the remote sensing community; however, further assessment of their performance to inform about plant function should be tested in different ecosystems. For example, the role of vertical and horizontal heterogeneity is still unclear. Robust evaluation, e.g. pattern-oriented model evaluation approach, would contribute to identify caveats and ecosystem-specific features that prevent accurate monitoring of their function; and that therefore, should be also represented.

Appendix A: Green fraction Neural Network predictor

In senSCOPE inversion, the fraction of green leaf area in the canopy (f_{green}) is estimated as a function of the canopy averaged leaf RTM parameters using a NN model trained form simulated data. Latin Hypercube Sampling was used to generate a look-up table (LUT) with 5000 samples of different leaf constituents (C_{ab}, C_{ant}, C_{dm}, C_w, C_s), N and f_{green}. C_{ca} was included in the LUT as a function of C_{ab} according to the relationship reported in Sims and Gamon (2002), and an uncertainty estimated in the relationship of ~4.5 µg cm^{-2} according to field measurements was used to add Gaussian noise. The same bounds that were applied in inversion (Section 3.3.2) were used to design the LUTs; however C_{ab} and C_{ca} of green leaves were limited to 40 and 10 µg cm^{-2}, respectively; according to field observations. LUT values were assumed to belong to pure green and senescent leaves, and averaged leaf parameters were mixed according with Eq. 21, assuming that in green leaves C_s = 0, and that in senescent leaves C_{ab} = 0, C_{ca} = 0, C_{ant} = 0. No additional assumptions about the values of the parameters of each leaf type and therefore the N, C_{dm}, C_w were taken directly from the LUT.

A NN was trained using SimpleR (Camps-Valls et al. 2012) to predict f_{green} as function of the canopy averaged leaf RTM parameters. During the training, 60 % of the dataset was used for fitting and 40 % for testing. Performance statistics are presented in Table A1.

Table A1. Statistics of the fraction green leaf area (f_{green}) Neural Network (NN) model.

Dataset	R^2	RMSE	ME	MAE
Training	0.818	0.123	0.005	0.093
Validation	0.718	0.230	0.158	0.180

Code availability

senSCOPE code and further developments, as well as the code for the multiple constraint inversion of the model are publicly available at https://github.com/JavierPachecoLabrador/senSCOPE.

Author contributions

JPL, TSEM, MM and CvdT designed the model. JPL and MM designed model evaluation. TSEM, AC, OPP, JG, PM, RGC, GM, MR and MM provided measurements of fluxes, plant parameters and spectral variables. JPL, CvdT, MM, OPP, JG, PM and RGC wrote the paper.

Acknowledgements

JPL, MM and MR acknowledge the EnMAP project MoReDEHESHyReS “Modelling Responses of Dehesas with Hyperspectral Remote Sensing” (Contract No. 50EE1621, German Aerospace Center (DLR) and the German Federal Ministry of Economic Affairs and Energy). Authors acknowledge the Alexander von Humboldt Foundation for supporting this research with the Max-Planck Prize to Markus Reichstein; the project SynerTGE “Landsat-8+Sent inel-2: exploring sensor synergies for monitoring and modelling key vegetation biophysical variables in tree-grass ecosystems” (CGL2015-69095-R, MINECO/FEDER,UE); and the project FLUχPEC “Monitoring changes in water and carbon fluxes from remote and proximal sensing in Mediterranean ‘dehesa’ ecosystem” (CGL2012-34383, Spanish Ministry of Economy and Competitiveness). Authors are very thankful to the MPI-BGC Freiland Group and especially Olaf Kolle, Martin Hertel as well as Ramón López-Jiménez (CEAM) for technical assistance. We are grateful to all the colleagues from MPI-BGC, University of Extremadura, University of Milano-Bicocca, SpecLab-CSIC, INIA and CEAM which have collaborated in any of the field and laboratory works. We acknowledge the Majadas de Tiétar city council for its support.

References

Anderson, R.C. (2006). Evolution and origin of the Central Grassland of North America: climate, fire, and mammalian grazers. *The Journal of the Torrey Botanical Society, 133*, 626-647, 622

Bach, H., Schneider, K., Verhoef, W., Stolz, R., Mauser, W., Van Leeuwen, H., Schouten, L., & Borgeaud, M. (2001). *Retrieval of geo-and biophysical information from remote sensing through advanced combination of a land surface process model with inversion techniques in the optical and microwave spectral range*.

881 Bach, H., & Verhoef, W. (2003). Sensitivity studies on the effect of surface soil moisture on canopy
882 reflectance using the radiative transfer model GeoSAIL. In, *IGARSS 2003. 2003 IEEE International*
883 *Geoscience and Remote Sensing Symposium. Proceedings (IEEE Cat. No.03CH37477)* (pp. 1679-1681)

884 Bacour, C., Jacquemoud, S., Leroy, M., Hautecœur, O., Weiss, M., Prévot, L., Bruguier, N., & Chauki,
885 H. (2002). Reliability of the estimation of vegetation characteristics by inversion of three canopy
886 reflectance models on airborne POLDER data. *Agronomie, 22*, 555-565

887 Bayat, B., van der Tol, C., & Verhoef, W. (2018). Integrating satellite optical and thermal infrared
888 observations for improving daily ecosystem functioning estimations during a drought episode. *Remote*
889 *Sensing of Environment, 209*, 375-394

890 Braswell, B.H., Schimel, D.S., Privette, J.L., Moore Iii, B., Emery, W.J., Sulzman, E.W., & Hudak,
891 A.T. (1996). Extracting ecological and biophysical information from AVHRR optical data: An
892 integrated algorithm based on inverse modeling. *Journal of Geophysical Research: Atmospheres, 101*,
893 23335-23348

894 Camino, C., Gonzalez-Dugo, V., Hernandez, P., & Zarco-Tejada, P.J. (2019). Radiative transfer Vcmax
895 estimation from hyperspectral imagery and SIF retrievals to assess photosynthetic performance in
896 rainfed and irrigated plant phenotyping trials. *Remote Sensing of Environment*, 111186

897 Camps-Valls, G., Munoz-Mari, J., Gomez-Chova, L., Guanter, L., & Calbet, X. (2012). Nonlinear
898 Statistical Retrieval of Atmospheric Profiles From MetOp-IASI and MTG-IRS Infrared Sounding Data.
899 *IEEE Transactions on Geoscience and Remote Sensing, 50*, 1759-1769

900 Castro, K.L., & Sanchez-Azofeifa, G.A. (2008). Changes in Spectral Properties, Chlorophyll Content
901 and Internal Mesophyll Structure of Senescing Populus balsamifera and Populus tremuloides Leaves.
902 *Sensors (Basel, Switzerland), 8*, 51-69

903 Cleland, E.E., Chiariello, N.R., Loarie, S.R., Mooney, H.A., & Field, C.B. (2006). Diverse responses of
904 phenology to global changes in a grassland ecosystem. *Proceedings of the National Academy of*
905 *Sciences, 103*, 13740

906 Croft, H., Chen, J.M., Luo, X., Bartlett, P., Chen, B., & Staebler, R.M. (2017). Leaf chlorophyll content
907 as a proxy for leaf photosynthetic capacity. *Global Change Biology, 23*, 3513-3524

908 Dash, J., & Curran, P.J. (2007). Evaluation of the MERIS terrestrial chlorophyll index (MTCI).
909 *Advances in Space Research, 39*, 100-104

910 Dutta, D., Schimel, D.S., Sun, Y., van der Tol, C., & Frankenberg, C. (2019). Optimal inverse
911 estimation of ecosystem parameters from observations of carbon and energy fluxes. *Biogeosciences, 16*,
912 77-103

913 El-Madany, T.S., Reichstein, M., Perez-Priego, O., Carrara, A., Moreno, G., Pilar Martín, M., Pacheco-
914 Labrador, J., Wohlfahrt, G., Nieto, H., Weber, U., Kolle, O., Luo, Y.-P., Carvalhais, N., & Migliavacca,
915 M. (2018). Drivers of spatio-temporal variability of carbon dioxide and energy fluxes in a
916 Mediterranean savanna ecosystem. *Agricultural and Forest Meteorology, 262*, 258-278

Feng, X., & Dietze, M. (2013). Scale dependence in the effects of leaf ecophysiological traits on photosynthesis: Bayesian parameterization of photosynthesis models. *New Phytologist, 200*, 1132-1144

Feret, J.-B., François, C., Asner, G.P., Gitelson, A.A., Martin, R.E., Bidel, L.P.R., Ustin, S.L., le Maire, G., & Jacquemoud, S. (2008). PROSPECT-4 and 5: Advances in the leaf optical properties model separating photosynthetic pigments. *Remote Sensing of Environment, 112*, 3030-3043

Féret, J.B. (2009). Apport de la modélisation pour l'estimation de la teneur en pigments foliaires par télédétection. In (p. 214): Université Pierre et Marie Curie

Féret, J.B., Gitelson, A.A., Noble, S.D., & Jacquemoud, S. (2017). PROSPECT-D: Towards modeling leaf optical properties through a complete lifecycle. *Remote Sensing of Environment, 193*, 204-215

Figueroa, M.E., & Davy, A.J. (1991). Response of Mediterranean Grassland Species to Changing Rainfall. *Journal of Ecology, 79*, 925-941

Frankenberg, C., & Berry, J. (2018). 3.10 - Solar Induced Chlorophyll Fluorescence: Origins, Relation to Photosynthesis and Retrieval A2 - Liang, Shunlin. *Comprehensive Remote Sensing* (pp. 143-162). Oxford: Elsevier

Friedlingstein, P., Meinshausen, M., Arora, V.K., Jones, C.D., Anav, A., Liddicoat, S.K., & Knutti, R. (2014). Uncertainties in CMIP5 Climate Projections due to Carbon Cycle Feedbacks. *Journal of Climate, 27*, 511-526

Gamon, J.A., & Berry, J.A. (2012). Facultative and constitutive pigment effects on the Photochemical Reflectance Index (PRI) in sun and shade conifer needles. *Israel Journal of Plant Sciences, 60*, 85-95

Gamon, J.A., Peñuelas, J., & Field, C.B. (1992). A narrow-waveband spectral index that tracks diurnal changes in photosynthetic efficiency. *Remote Sensing of Environment, 41*, 35-44

Garbulsky, M.F., Peñuelas, J., Gamon, J., Inoue, Y., & Filella, I. (2011). The photochemical reflectance index (PRI) and the remote sensing of leaf, canopy and ecosystem radiation use efficiencies: A review and meta-analysis. *Remote Sensing of Environment, 115*, 281-297

Golub, G.H., & Loan, C.F.v. (1980). An Analysis of the Total Least Squares Problem. *SIAM Journal on Numerical Analysis, 17*, 883-893

Gonzalez-Cascon, R., Jiménez-Fenoy, L., Verdú-Fillola, I., & Martín, M.P. (2017). Short communication: Aqueous-acetone extraction improves the drawbacks of using dimethylsulfoxide as solvent for photometric pigment quantification in Quercus ilex leaves. *2017, 26*

Gonzalez-Cascon, R., & Martin, M.P. (2018). Protocol for pigment content quantification in herbaceous covers: sampling and analysis, *October 2019*

Guyot, S., Vercauteren, J., & Cheynier, V. (1996). Structural determination of colourless and yellow dimers resulting from (+)-catechin coupling catalysed by grape polyphenoloxidase. *Phytochemistry, 42*, 1279-1288

He, Y., & Mui, A. (2010). Scaling up Semi-Arid Grassland Biochemical Content from the Leaf to the Canopy Level: Challenges and Opportunities. *Sensors, 10*, 11072-11087

Henry, H.A.L., Brizgys, K., & Field, C.B. (2008). Litter Decomposition in a California Annual Grassland: Interactions Between Photodegradation and Litter Layer Thickness. *Ecosystems, 11*, 545-554

Hörtensteiner, S. (2006). CHLOROPHYLL DEGRADATION DURING SENESCENCE. *Annual Review of Plant Biology, 57*, 55-77

Houborg, R., & Anderson, M. (2009). Utility of an image-based canopy reflectance modeling tool for remote estimation of LAI and leaf chlorophyll content at regional scales. In (p. 29): SPIE

Houborg, R., Anderson, M., & Daughtry, C. (2009). Utility of an image-based canopy reflectance modeling tool for remote estimation of LAI and leaf chlorophyll content at the field scale. *Remote Sensing of Environment, 113*, 259-274

Houborg, R., & Boegh, E. (2008). Mapping leaf chlorophyll and leaf area index using inverse and forward canopy reflectance modeling and SPOT reflectance data. *Remote Sensing of Environment, 112*, 186-202

Houborg, R., McCabe, M., Cescatti, A., Gao, F., Schull, M., & Gitelson, A. (2015). Joint leaf chlorophyll content and leaf area index retrieval from Landsat data using a regularized model inversion system (REGFLEC). *Remote Sensing of Environment, 159*, 203-221

Houborg, R., & McCabe, M.F. (2016). Adapting a regularized canopy reflectance model (REGFLEC) for the retrieval challenges of dryland agricultural systems. *Remote Sensing of Environment, 186*, 105-120

IPCC (2014). Climate Change 2014: Synthesis Report. Contribution of Working Groups I, II and III to the Fifth Assessment Report of the Intergovernmental Panel on Climate Change. In R.K.P.a.L.A. Meyer (Ed.) (p. 151). Geneva, Switzerland: IPCC

Jacquemoud, S. (1988). Modélisation des propriétés optiques des feuilles. In: USTL / ENSA Montpellier / INRA

Jacquemoud, S., & Baret, F. (1990). PROSPECT: A model of leaf optical properties spectra. *Remote Sensing of Environment, 34*, 75-91

Jacquemoud, S., Verhoef, W., Baret, F., Bacour, C., Zarco-Tejada, P.J., Asner, G.P., François, C., & Ustin, S.L. (2009). PROSPECT+SAIL models: A review of use for vegetation characterization. *Remote Sensing of Environment, 113*, S56-S66

Kidnie, S., Cruz, M.G., Gould, J., Nichols, D., Anderson, W., & Bessell, R. (2015). Effects of curing on grassfires: I. Fuel dynamics in a senescing grassland. *International Journal of Wildland Fire, 24*, 828-837

Koukoura, Z., Mamolos, A.P., & Kalburtji, K.L. (2003). Decomposition of dominant plant species litter in a semi-arid grassland. *Applied Soil Ecology, 23*, 13-23

Luo, Y., El-Madany, T., Filippa, G., Ma, X., Ahrens, B., Carrara, A., Gonzalez-Cascon, R., Cremonese, E., Galvagno, M., Hammer, T., Pacheco-Labrador, J., Martín, M., Moreno, G., Perez-Priego, O., Reichstein, M., Richardson, A., Römermann, C., & Migliavacca, M. (2018). Using Near-Infrared-Enabled Digital Repeat Photography to Track Structural and Physiological Phenology in Mediterranean Tree–Grass Ecosystems. *Remote Sensing, 10*, 1293

Martín, M.P., Pacheco-Labrador, J., Gonzalez-Cascon, R., Moreno, G., Migliavacca, M., García, M., Yebra, M., & Riaño, D. (2019). Estimación de variables esenciales de la vegetación en un ecosistema de dehesa utilizando factores de reflectividad simulados con PROSAIL + FLIGHT. In A.E.d. Teledetección (Ed.), *XVIII Congreso Nacional de Teledetección*. Valladolid, Spain, 24-27 September 2019

Martini, D., Pacheco-Labrador, J., Perez-Priego, O., van der Tol, C., El-Madany, S.T., Julitta, T., Rossini, M., Reichstein, M., Christiansen, R., Rascher, U., Moreno, G., Martín, P.M., Yang, P., Carrara, A., Guan, J., González-Cascón, R., & Migliavacca, M. (2019). Nitrogen and Phosphorus Effect on Sun-Induced Fluorescence and Gross Primary Productivity in Mediterranean Grassland. *Remote Sensing, 11*

McKay, M.D., Beckman, R.J., & Conover, W.J. (1979). A Comparison of Three Methods for Selecting Values of Input Variables in the Analysis of Output from a Computer Code. *Technometrics, 21*, 239-245

Melendo-Vega, J., Martín, M., Pacheco-Labrador, J., González-Cascón, R., Moreno, G., Pérez, F., Migliavacca, M., García, M., North, P., & Riaño, D. (2018). Improving the Performance of 3-D Radiative Transfer Model FLIGHT to Simulate Optical Properties of a Tree-Grass Ecosystem. *Remote Sensing, 10*, 2061

Migliavacca, M., Galvagno, M., Cremonese, E., Rossini, M., Meroni, M., Sonnentag, O., Cogliati, S., Manca, G., Diotri, F., Busetto, L., Cescatti, A., Colombo, R., Fava, F., Morra di Cella, U., Pari, E., Siniscalco, C., & Richardson, A.D. (2011). Using digital repeat photography and eddy covariance data to model grassland phenology and photosynthetic CO2 uptake. *Agricultural and Forest Meteorology, 151*, 1325-1337

Migliavacca, M., Perez-Priego, O., Rossini, M., El-Madany, T.S., Moreno, G., van der Tol, C., Rascher, U., Berninger, A., Bessenbacher, V., Burkart, A., Carrara, A., Fava, F., Guan, J.-H., Hammer, T.W., Henkel, K., Juarez-Alcalde, E., Julitta, T., Kolle, O., Martín, M.P., Musavi, T., Pacheco-Labrador, J., Pérez-Burgueño, A., Wutzler, T., Zaehle, S., & Reichstein, M. (2017). Plant functional traits and canopy structure control the relationship between photosynthetic CO2 uptake and far-red sun-induced fluorescence in a Mediterranean grassland under different nutrient availability. *New Phytologist, 214*, 1078-1091

Omlin, M., & Reichert, P. (1999). A comparison of techniques for the estimation of model prediction uncertainty. *Ecological Modelling, 115*, 45-59

Pacheco-Labrador, J., El-Madany, T., Martín, M., Migliavacca, M., Rossini, M., Carrara, A., & Zarco-Tejada, P.J. (2017). Spatio-Temporal Relationships between Optical Information and Carbon Fluxes in a Mediterranean Tree-Grass Ecosystem. *Remote Sensing, 9*, 608

Pacheco-Labrador, J., Perez-Priego, O., El-Madany, T.S., Julitta, T., Rossini, M., Guan, J., Moreno, G., Carvalhais, N., Martín, M.P., Gonzalez-Cascon, R., Kolle, O., Reischtein, M., van der Tol, C., Carrara, A., Martini, D., Hammer, T.W., Moossen, H., & Migliavacca, M. (2019). Multiple-constraint inversion of SCOPE. Evaluating the potential of GPP and SIF for the retrieval of plant functional traits. *Remote Sensing of Environment, 234*, 111362

Perez-Priego, O., El-Madany, T.S., Migliavacca, M., Kowalski, A.S., Jung, M., Carrara, A., Kolle, O., Martín, M.P., Pacheco-Labrador, J., Moreno, G., & Reichstein, M. (2017). Evaluation of eddy covariance latent heat fluxes with independent lysimeter and sapflow estimates in a Mediterranean savannah ecosystem. *Agricultural and Forest Meteorology, 236*, 87-99

Perez-Priego, O., Guan, J., Rossini, M., Fava, F., Wutzler, T., Moreno, G., Carvalhais, N., Carrara, A., Kolle, O., Julitta, T., Schrumpf, M., Reichstein, M., & Migliavacca, M. (2015). Sun-induced chlorophyll fluorescence and photochemical reflectance index improve remote-sensing gross primary production estimates under varying nutrient availability in a typical Mediterranean savanna ecosystem. *Biogeosciences, 12*, 6351-6367

Porcar-Castell, A., Tyystjärvi, E., Atherton, J., van der Tol, C., Flexas, J., Pfündel, E.E., Moreno, J., Frankenberg, C., & Berry, J.A. (2014). Linking chlorophyll a fluorescence to photosynthesis for remote sensing applications: mechanisms and challenges. *Journal of Experimental Botany, 65*, 4065-4095

Pourcel, L., Routaboul, J.-M., Cheynier, V., Lepiniec, L., & Debeaujon, I. (2007). Flavonoid oxidation in plants: from biochemical properties to physiological functions. *Trends in Plant Science, 12*, 29-36

Ren, H., & Zhang, B. (2018). Spatiotemporal variations in litter mass and their relationships with climate in temperate grassland: A case study from Xilingol grassland, Inner Mongolia (China). *Advances in Space Research, 61*, 1055-1065

Richardson, A.D., Keenan, T.F., Migliavacca, M., Ryu, Y., Sonnentag, O., & Toomey, M. (2013). Climate change, phenology, and phenological control of vegetation feedbacks to the climate system. *Agricultural and Forest Meteorology, 169*, 156-173

Rogers, A. (2014). The use and misuse of V c,max in Earth System Models. *Photosynthesis Research, 119*, 15-29

Rogers, A., Medlyn Belinda, E., Dukes Jeffrey, S., Bonan, G., Caemmerer, S., Dietze Michael, C., Kattge, J., Leakey Andrew, D.B., Mercado Lina, M., Niinemets, Ü., Prentice, I.C., Serbin Shawn, P., Sitch, S., Way Danielle, A., & Zaehle, S. (2016). A roadmap for improving the representation of photosynthesis in Earth system models. *New Phytologist, 213*, 22-42

Rouse, J.W., Haas, R.H., Schell, J.A., & Deering, D.W. (1974). Monitoring vegetation systems in the Great Plains with ERTS. In S.C. Freden, E.P. Mercanti, & M.A. Becker (Eds.), *Third Earth Resources Technology Satellite- 1 Symposium* (pp. 301–317). Greenbelt, MD, USA: NASA

Sanaullah, M., Chabbi, A., Lemaire, G., Charrier, X., & Rumpel, C. (2010). How does plant leaf senescence of grassland species influence decomposition kinetics and litter compounds dynamics? *Nutrient Cycling in Agroecosystems, 88*, 159-171

Schaefer, K., Schwalm Christopher, R., Williams, C., Arain, M.A., Barr, A., Chen Jing, M., Davis Kenneth, J., Dimitrov, D., Hilton Timothy, W., Hollinger David, Y., Humphreys, E., Poulter, B., Raczka Brett, M., Richardson Andrew, D., Sahoo, A., Thornton, P., Vargas, R., Verbeeck, H., Anderson, R., Baker, I., Black, T.A., Bolstad, P., Chen, J., Curtis Peter, S., Desai Ankur, R., Dietze, M., Dragoni, D., Gough, C., Grant Robert, F., Gu, L., Jain, A., Kucharik, C., Law, B., Liu, S., Lokipitiya, E., Margolis Hank, A., Matamala, R., McCaughey, J.H., Monson, R., Munger, J.W., Oechel, W., Peng, C., Price David, T., Ricciuto, D., Riley William, J., Roulet, N., Tian, H., Tonitto, C., Torn, M., Weng, E., & Zhou, X. (2012). A model-data comparison of gross primary productivity: Results from the North American Carbon Program site synthesis. *Journal of Geophysical Research: Biogeosciences, 117*

Serbin, S.P., Singh, A., Desai, A.R., Dubois, S.G., Jablonski, A.D., Kingdon, C.C., Kruger, E.L., & Townsend, P.A. (2015). Remotely estimating photosynthetic capacity, and its response to temperature, in vegetation canopies using imaging spectroscopy. *Remote Sensing of Environment, 167*, 78-87

Silva-Perez, V., Molero, G., Serbin, S.P., Condon, A.G., Reynolds, M.P., Furbank, R.T., & Evans, J.R. (2018). Hyperspectral reflectance as a tool to measure biochemical and physiological traits in wheat. *Journal of Experimental Botany, 69*, 483-496

Sims, D.A., & Gamon, J.A. (2002). Relationships between leaf pigment content and spectral reflectance across a wide range of species, leaf structures and developmental stages. *Remote Sensing of Environment, 81*, 337-354

Taranto, F., Pasqualone, A., Mangini, G., Tripodi, P., Miazzi, M.M., Pavan, S., & Montemurro, C. (2017). Polyphenol Oxidases in Crops: Biochemical, Physiological and Genetic Aspects. *International Journal of Molecular Sciences, 18*, 377

van der Tol, C., Rossini, M., Cogliati, S., Verhoef, W., Colombo, R., Rascher, U., & Mohammed, G. (2016). A model and measurement comparison of diurnal cycles of sun-induced chlorophyll fluorescence of crops. *Remote Sensing of Environment, 186*, 663-677

van der Tol, C., Verhoef, W., Timmermans, J., Verhoef, A., & Su, Z. (2009). An integrated model of soil-canopy spectral radiances, photosynthesis, fluorescence, temperature and energy balance. *Biogeosciences, 6*, 3109-3129

Verhoef, W. (1984). Light scattering by leaf layers with application to canopy reflectance modeling: The SAIL model. *Remote Sensing of Environment, 16*, 125-141

Verhoef, W., & Bach, H. (2003). Remote sensing data assimilation using coupled radiative transfer models. *Physics and Chemistry of the Earth, Parts A/B/C, 28*, 3-13

Verhoef, W., van der Tol, C., & Middleton, E.M. (2018). Hyperspectral radiative transfer modeling to explore the combined retrieval of biophysical parameters and canopy fluorescence from FLEX – Sentinel-3 tandem mission multi-sensor data. *Remote Sensing of Environment, 204*, 942-963

Vilfan, N., van der Tol, C., Muller, O., Rascher, U., & Verhoef, W. (2016). Fluspect-B: A model for leaf fluorescence, reflectance and transmittance spectra. *Remote Sensing of Environment, 186*, 596-615

Vilfan, N., Van der Tol, C., Yang, P., Wyber, R., Malenovský, Z., Robinson, S.A., & Verhoef, W. (2018). Extending Fluspect to simulate xanthophyll driven leaf reflectance dynamics. *Remote Sensing of Environment, 211*, 345-356

Wang, Q., Tenhunen, J., Dinh, N.Q., Reichstein, M., Otieno, D., Granier, A., & Pilegarrd, K. (2005). Evaluation of seasonal variation of MODIS derived leaf area index at two European deciduous broadleaf forest sites. *Remote Sensing of Environment, 96*, 475-484

Wenhan, Q. (1993). Modeling bidirectional reflectance of multicomponent vegetation canopies. *Remote Sensing of Environment, 46*, 235-245

Whitfield, D.M., & Rowan, K.S. (1974). Changes in the chlorophylls and carotenoids of leaves of Nicotiana tabacum during senescence. *Phytochemistry, 13*, 77-83

Yang, P., Verhoef, W., & van der Tol, C. (2017). The mSCOPE model: A simple adaptation to the SCOPE model to describe reflectance, fluorescence and photosynthesis of vertically heterogeneous canopies. *Remote Sensing of Environment, 201*, 1-11

Yuan, Z., & Chen, H.Y.H. (2009). Global trends in senesced-leaf nitrogen and phosphorus. *Global Ecology and Biogeography, 18*, 532-542

Zhang, Y., Guanter, L., Berry Joseph, A., Joiner, J., Tol, C., Huete, A., Gitelson, A., Voigt, M., & Köhler, P. (2014). Estimation of vegetation photosynthetic capacity from space-based measurements of chlorophyll fluorescence for terrestrial biosphere models. *Global Change Biology, 20*, 3727-3742

Zhang, Y., Guanter, L., Joiner, J., Song, L., & Guan, K. (2018). Spatially-explicit monitoring of crop photosynthetic capacity through the use of space-based chlorophyll fluorescence data. *Remote Sensing of Environment, 210*, 362-374